# Paleotemperature and paleosalinity inferences and chemostratigraphy across the Aptian/Albian boundary in the subtropical North Atlantic

Brian T. Huber,[1] Kenneth G. MacLeod,[2] Darren R. Gröcke,[3] and Michal Kucera[4]

Received 31 May 2011; revised 13 September 2011; accepted 9 October 2011; published 21 December 2011.

[1] Geochemical analyses of extraordinarily well preserved late Aptian–early Albian foraminifera from Blake Nose (Ocean Drilling Program Site 1049) reveal rapid shifts of $\delta^{18}O$, $\delta^{13}C$, and $^{87}Sr/^{88}Sr$ in the subtropical North Atlantic that may be linked to a major planktic foraminifer extinction event across the Aptian/Albian boundary. The abruptness of the observed geochemical shifts and their coincidence with a sharp lithologic contact is explained as an artifact of a previously undetected hiatus of 0.8–1.4 million years at the boundary contact, but the values before and after the hiatus indicate that major oceanographic changes occurred at this time. $^{87}Sr/^{88}Sr$ increase by ~0.000 200, $\delta^{13}C$ values decrease by 1.5‰ to 2.2‰, and $\delta^{18}O$ values decrease by ~1.0‰ (planktics) to 0.5‰ (benthics) across the hiatus. Further, both $^{87}Sr/^{88}Sr$ ratios and $\delta^{18}O$ values during the Albian are anomalously high. The $^{87}Sr/^{88}Sr$ values deviate from known patterns to such a degree that an explanation requires either the presence of inter-basin differences in seawater $^{87}Sr/^{88}Sr$ during the Albian or revision of the seawater curve. For $\delta^{18}O$, planktic values in some Aptian samples likely reflect a diagenetic overprint, but preservation is excellent in the rest of the section. In well preserved material, benthic foraminiferal values are largely between 0.5 and 0.0‰ and planktic samples are largely between 0.0‰ to −1.0‰, with a brief excursion to −2.0‰ during OAE 1b. Using standard assumptions for Cretaceous isotopic paleotemperature calculations, the $\delta^{18}O$ values suggest bottom water temperatures (at ~1000 –1500 m) of 8–10°C and surface temperatures of 10–14°C, which are 4–6°C and 10–16°C cooler, respectively, than present-day conditions at the same latitude. The cool subtropical sea surface temperature estimates are especially problematic because other paleoclimate proxy data for the mid-Cretaceous and climate model predictions suggest that subtropical sea surface temperatures should have been the same as or warmer than at present. Because of their exquisite preservation, whole scale alteration of the analyzed foraminifera is an untenable explanation. Our proposed solution is a high evaporative fractionation factor in the early Albian North Atlantic that resulted in surface waters with higher $\delta^{18}O$ values at elevated salinities than commonly cited in Cretaceous studies. A high fractionation factor is consistent with high rates of vapor export and a vigorous hydrological cycle and, like the Sr isotopes, implies limited connectivity among the individual basins of the Early Cretaceous proto-Atlantic ocean.

**Citation:** Huber, B. T., K. G. MacLeod, D. R. Gröcke, and M. Kucera (2011), Paleotemperature and paleosalinity inferences and chemostratigraphy across the Aptian/Albian boundary in the subtropical North Atlantic, *Paleoceanography*, *26*, PA4221, doi:10.1029/2011PA002178.

## 1. Introduction

[2] One of the most significant turnover events in the evolutionary history of planktic foraminifera occurs across the Aptian–Albian boundary interval [*Premoli Silva and Sliter*, 1999; *Leckie et al.*, 2002; *Huber and Leckie*, 2011a]. However, problems with ambiguous or incorrect planktic foraminiferal identifications, limited biostratigraphic resolution, scarcity of stratigraphically complete successions, and moderate to severe diagenetic overprints have long hindered detailed documentation of changes in species composition, as well as geochemical investigations of the paleoceanography

[1]Smithsonian National Museum of Natural History, Washington, District of Columbia, USA.
[2]Department of Geological Sciences, University of Missouri, Columbia, Missouri, USA.
[3]Department of Earth Sciences, Durham University, Durham, UK.
[4]Fachbereich Geowissenschaften, Eberhard-Karls Universität Tübingen, Tübingen, Germany.


0883-8305/11/2011PA002178

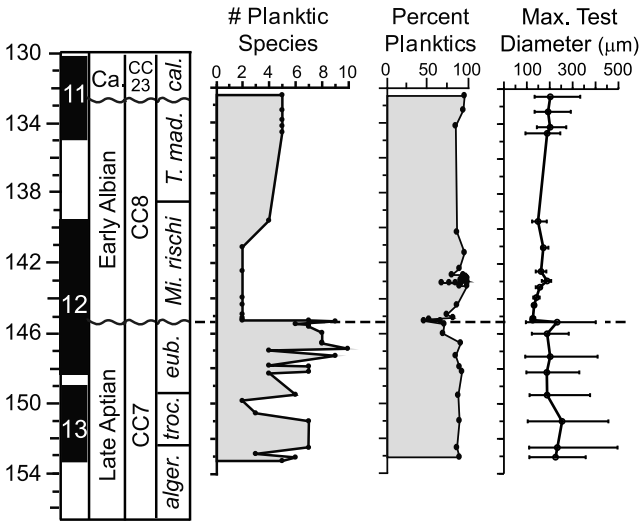


**Figure 1.** Changes in number of planktic foraminiferal species, percent planktic abundance relative to total planktic and benthic specimens, and maximum diameter of planktic foraminiferal tests across the Aptian/Albian boundary interval of ODP Hole 1049C based on the study of *Huber and Leckie* [2011a].

and paleoclimatology of this time interval. For these reasons, the extent of the extinction event and the paleoceanographic changes associated with it remained largely unknown.

[3] Study of extraordinarily well preserved foraminifera from Ocean Drilling Program (ODP) Site 1049 (subtropical North Atlantic) and Deep Sea Drilling Project (DSDP) Site 511 (southern South Atlantic) and restudy of several other deep-sea sections by *Huber and Leckie* [2011a] has resolved a number of biostratigraphic and taxonomic discrepancies and has led to the recognition that the Aptian/Albian extinction was more abrupt and of greater magnitude than had been previously recognized (Figure 1). Using the highest occurrence (HO) of the Aptian planktic foraminifer *Paraticinella eubejaouaensis* to identify the top of the Aptian Stage, these authors observed (1) an extinction rate of about 70 to 80% of the Aptian species with a loss of all large-sized (200–700 $\mu$m) species with thick-walled shells bearing a distinctive pore mound ornamentation; (2) a precipitous drop in the planktic to-benthic-ratio correlated with the planktic species extinction; (3) a sparse earliest Albian planktic fauna consisting of only two very small-sized (100–130 $\mu$m) species with thin walled tests that bear little or no surface ornamentation; and (4) a gradual increase in species diversity and maximum shell diameter through the ~13 million yearlong Albian Age.

[4] A cool global climate during the late Aptian and early Albian has been inferred from the presence of dropstones and glendonites in southern Australia and Arctic Canada [*Kemper*, 1987; *Frakes et al.*, 1992; *Price*, 1999], relatively high $\delta^{18}$O values in concretion cements from fluvial sediments in southeast Australia [*Ferguson et al.*, 1999], stable isotope analyses of bulk marine carbonate [*Clarke and Jenkyns*, 1999] and belemnites from Australia and Argentina [*Pirrie et al.*, 1995, 2004]. Negative shifts in carbon isotope records from bulk marine carbonates and a drop in global sea level were interpreted as evidence for growth of a continental ice sheet at this time [*Weissert and Lini*, 1991]. However, these paleoclimatic inferences provide only broad paleotemperature constraints and there are few data spanning the Aptian–Albian boundary interval.

[5] A major impediment to producing $\delta^{18}$O-based paleotemperature estimates for the Early Cretaceous has been carbonate preservation. Most shells of this age are encased in limestone, infilled with secondary calcium carbonate, overgrown with euhedral inorganic calcite crystals, or strongly recrystallized. Although oxygen isotope values from apparently unaltered belemnite guards have been used in sea-surface paleotemperature estimations [e.g., *Sellwood et al.*, 1994; *Pirrie et al.*, 1995, 2004], comparison between oxygen and carbon isotope ratios from Antarctic belemnites and co-occurring benthic and planktic foraminifera indicates that belemnites lived below the surface summer mixed layer and so do not record sea surface temperatures [*Dutton et al.*, 2007].

[6] The presence of exceptionally well-preserved, translucent ('glassy') foraminifera in the Aptian–Albian boundary interval (~115–108 Ma) at Site 1049 provides a rare opportunity to address this shortcoming. The primary objectives for this study are to: (1) document $\delta^{18}$O and $\delta^{13}$C trends using monospecific planktic and benthic foraminifer and bulk carbonate samples; (2) evaluate standard assumptions for the oxygen isotopic composition of Cretaceous seawater used to calculate water temperatures relative to the new results; (3) obtain $^{87}$Sr/$^{86}$Sr ratio data across the Site 1049 Aptian/Albian boundary to constrain the duration of the apparent hiatus; (4) correlate the bulk carbonate and foraminifer carbon isotope curves obtained from Site 1049 with the standard reference $\delta^{13}$C curve developed for the late Aptian–early Albian in the Vocontian Basin [*Herrle et al.*, 2004]; and (5) establish a microfossil-based age model for calculation of sedimentation rates and estimation of the duration of an unconformity across the Aptian/Albian boundary.

## 2. Geologic Setting and Species Turnover at Site 1049

[7] Site 1049 was drilled on Blake Plateau at 2,670 m water depth about 530 km east of Jacksonville, Florida (30°8.53′N, 76°6.72′W, Figure 2). The site is positioned at Blake Nose which lies at the outer flank of a gently sloping ramp with Paleogene and Cretaceous strata that deepen and thin eastward. During the late Aptian–early Albian the site was located about 60 km seaward of a large carbonate platform that ran parallel to the present-day Florida coast [*Norris et al.*, 1998]. Paleodepth estimates range from middle bathyal [*Norris et al.*, 1998] to outer shelf to upper slope [*Holbourn and Kuhnt*, 2001]. Paleomagnetics suggest a paleolatitude of ~25°N from the mid-Cretaceous through Eocene [*Ogg and Bardot*, 2001].

[8] The Upper Aptian–Lower Albian at Site 1049 is ~32 m thick and composed dominantly of rhythmically alternating red, white and green bioturbated calcareous clay and clay-rich chalk [*Benson et al.*, 1978; *Norris et al.*, 1998]. A finely laminated, 46 cm thick black shale containing up to 12.3 wt % total organic carbon [*Barker et al.*, 2001] was recovered from the lower Albian *Microhedbergella rischi* Zone at each of the three Site 1049 drill holes. This level has been identified as the regional expression of OAE 1b and was correlated

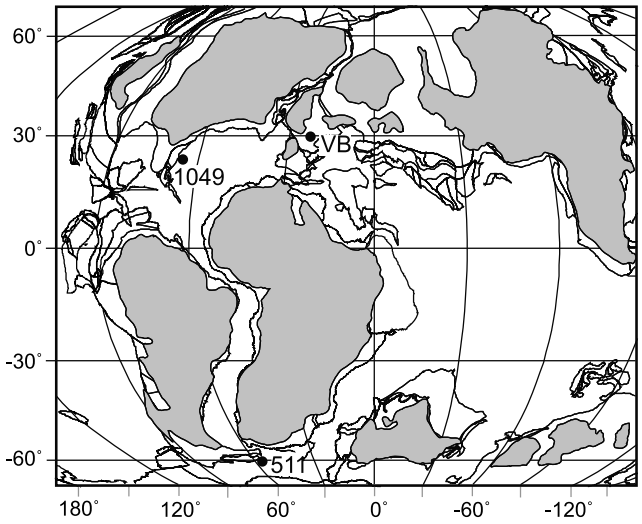


**Figure 2.** Paleogeographic reconstruction for 112 Ma based on work by *Hay et al.* [1999] showing location of Aptian/Albian boundary DSDP and ODP sites and Vocontian Basin (VB) Pré-Guittard section that are discussed in this study.

with the Niveau Paquier in the Vocontian Basin [*Erbacher et al*., 2001; *Trabucho Alexandre et al.*, 2011]. The black shale sediments are interpreted as having resulted from a major increase in the contribution of $^{13}$C-enriched organic carbon derived from chemoautotrophic marine archaea that flourished in a well stratified, low-temperature water column [*Kuypers et al.*, 2001].

[9] The Aptian/Albian boundary is placed 2.16 m below the OAE 1b black shale in Holes 1049A and 1049C, but in Hole 1049B it occurs in a coring gap. The boundary is identified at the extinction of the distinctive Aptian biomarker *Pa. eubejaouaensis*, which occurs just below a sharp contact between a white calcareous chalk and an overlying gray calcareous claystone. The white chalk interval below the lithologic contact is interpreted as latest Aptian in age based on the presence of specimens of evolutionarily advanced forms of *Pa. eubejaouaensis* (sensu *Premoli Silva et al.* [2009]). Species diversity drops from a peak of 11 planktic species in a sample 1.22 m below the boundary to 7 species 5 cm below the boundary. The overlying gray claystone contains none of the late Aptian species and only two small early Albian species *Microhedbergella rischi* and *Mi. renilaevis*. The 80% decrease in species richness is accompanied by an abrupt 50% decrease in mean shell diameter and a 40% increase in the percentage of benthic species (Figure 1). The boundary at Site 1049 has been interpreted as an unconformity based on the sharp lithologic contact and the lack of transitional planktic foraminiferal species seen in the earliest Albian in other boundary sections [*Huber and Leckie*, 2011a].

## 3. Material and Methods

### 3.1. Samples

[10] Samples for this study were collected from the Bremen Core Repository at the University of Bremen, and are identified using standard IODP "hole, core-section, interval" conventions. Sample depths are reported as meters below seafloor (mbsf). Samples processed at Royal Holloway University in London (RHUL) were soaked in deionized water and agitated on an orbital shaker overnight. Samples processed at the Smithsonian Institution (SI) were soaked for 24 h in tap water. The samples were then washed over a 63 $\mu$m sieve until the residue was free of adhering clay and fine particles and then dried at 50°C. The biostratigraphic framework used follows *Huber and Leckie* [2011a]; ages for stage and biozone boundaries are from work by *Gradstein et al.* [2004].

### 3.2. Stable Isotope Analyses

[11] Oxygen and carbon isotopic ratios were measured on single species benthic and planktic foraminiferal separates across a 21 m interval from the upper Aptian *Globigerinelloides algerianus* Zone to the lower Albian *Ticinella madecassiana* Zone in Hole 1049C. At least one trochospiral benthic species and two to six co-occurring planktic species were selected from each sample, with care taken to ensure analysis of the best preserved and largest sized specimens for each species in each sample. To test for reworking in the immediate boundary interval, two benthic species and six planktic species were analyzed from four additional samples across a 16 cm interval from Hole 1049A that straddles the Aptian/Albian boundary. Typically 25 to 80 specimens were analyzed for the smaller-sized species (<150 $\mu$m maximum dimension; e.g., *Microhedbergella* spp., *Pseudoguembelitria blakenosensis*), whereas 1 to 4 specimens were analyzed for larger-sized species (>350 $\mu$m maximum dimension; e.g., *Pa. eubejaouaensis*). Sample spacing for the single species separates ranges from 2 cm to 1.5 m with closer spacing near the Aptian/Albian boundary interval. In addition, 212 bulk analyses were run on samples spanning the studied interval in Hole 1049C (sample spacing of ~10 cm throughout).

[12] Samples were run at several labs (Tables 1–4) and all are reported using standard delta ($\delta$) notation and the Vienna PDB (VPDB) scale. The University of Missouri uses a Kiel III automated carbonate device coupled with a Thermo Finnigan™ DeltaPlus IRMS. Results were normalized within each run by the difference between within-run average of replicate analyses of NBS-19 (typically six) and nominal values of −2.20‰ and +1.95‰ for $\delta^{18}$O and $\delta^{13}$C, respectively. Long-term precision (1 SD) of the standard analyses (uncorrected) is <0.06‰ for $\delta^{18}$O and <0.03‰ for $\delta^{13}$C. At McMaster University the bulk carbonate record was produced using a common-acid bath system. For samples run at the RHUL, individual foraminifera were hand-picked until enough carbonate for isotopic analysis was obtained (typically 200 $\mu$g). Samples were weighed into individual, septum sealed vials and positioned in a hot plate set at 90°C. Each vial was flushed with helium to remove any air before $H_3PO_4$ was added. The samples remained in this condition for ~1 h to enable equilibration to occur after which the liberated $CO_2$ gas was analyzed under continuous helium flow connected to a Micromass Isoprime mass spectrometer. All samples were corrected using the NBS-19 international standard ($\delta^{13}$C = +1.95%, $\delta^{18}$O = −2.20%). The analytical precision of this standard was better than 0.1% for both $\delta^{13}$C and $\delta^{18}$O. Sample reproducibility was generally better than 0.2‰ based on duplicate sample analysis.

**Table 1.** Aptian Oxygen and Carbon Isotope Data for Bulk Carbonate and Foraminifera Samples Obtained From ODP Hole 1049C, Analyzed at the University of Missouri Stable Isotope Facility[a]

| Hole 1049C Sample | Depth[b] (mbsf) | Biozone | *Berthelina* spp. | | *Gl. aptiensis* | | *Gl. ferreol.* | | *Gl. algerian.* | | *Ps. cheniour.* | | *Pa. eubejaou.* | | *Hd. occulta* | | *Pg. blakenos.* | | *Hd. infracret.* | | *Hd. trocoid.* | | *Hd. aptiana* | |
|---|---|---|---|---|---|---|---|---|---|---|---|---|---|---|---|---|---|---|---|---|---|---|---|---|
| | | | $\delta^{13}C$ | $\delta^{18}O$ | $\delta^{13}C$ | $\delta^{18}O$ | $\delta^{13}C$ | $\delta^{18}O$ | $\delta^{13}C$ | $\delta^{18}O$ | $\delta^{13}C$ | $\delta^{18}O$ | $\delta^{13}C$ | $\delta^{18}O$ | $\delta^{13}C$ | $\delta^{18}O$ | $\delta^{13}C$ | $\delta^{18}O$ | $\delta^{13}C$ | $\delta^{18}O$ | $\delta^{13}C$ | $\delta^{18}O$ | $\delta^{13}C$ | $\delta^{18}O$ |
| 12X-4, 140–142 | 145.21 | *Micro. rischi* | | | | | | | | | | | 3.64 | −0.02 | | | | | | | | | | |
| 12X-4, 145–147 | 145.26 | *Para. eubej.* | 1.33 | 0.17 | | | | | | | | | 3.40 | −0.32 | | | | | | | | | 2.15 | −0.07 |
| 12X-4, 149–150 | 145.29 | *Para. eubej.* | 2.66 | 0.76 | | | | | | | | | 3.22 | −0.29 | | | | | | | | | 2.86 | 0.48 |
| 12X-5, 0–2 | 145.31 | *Para. eubej.* | 3.18 | 0.59 | | | | | | | | | 3.41 | −0.21 | | | | | | | | | 3.58 | 0.89 |
| 12X-5, 0–2 | 145.31 | *Para. eubej.* | | | | | | | | | | | | | | | | | | | | | 2.80 | 0.47 |
| 12X-5, 5–7 | 145.36 | *Para. eubej.* | 2.99 | 0.74 | | | | | | | | | 3.84 | 0.10 | | | | | | | | | 2.60 | 0.32 |
| 12X-5, 10–12 | 145.41 | *Para. eubej.* | 3.09 | 0.78 | | | | | | | | | 3.93 | 0.04 | | | | | | | | | 3.82 | 1.12 |
| 12X-5, 20–22 | 145.51 | *Para. eubej.* | 2.91 | 0.56 | | | | | | | | | 3.87 | 0.08 | | | | | | | | | | |
| 12X-5, 30–32 | 145.61 | *Para. eubej.* | 2.75 | 0.59 | | | | | | | | | 3.81 | 0.06 | | | 3.49 | 1.06 | | | | | | |
| 12X-5, 39–40 | 145.69 | *Para. eubej.* | 2.84 | 0.49 | | | | | | | | | 3.82 | 0.09 | | | | | | | | | 3.71 | 1.04 |
| 12X-5, 50–51 | 145.80 | *Para. eubej.* | 3.30 | 0.72 | | | | | | | | | 4.11 | 0.19 | | | | | | | | | 4.05 | 0.94 |
| 12X-5, 69–70 | 145.99 | *Para. eubej.* | 3.02 | 0.72 | | | | | | | | | 4.05 | 0.08 | 4.05 | 0.11 | 4.03 | 0.78 | 4.01 | 0.23 | 3.98 | 0.00 | | |
| 12X-5, 109–110 | 146.39 | *Para. eubej.* | 2.95 | 0.59 | | | 3.87 | 0.78 | | | | | 4.06 | 0.29 | | | | | | | | | | |
| 12X-5, 130–131 | 146.60 | *Para. eubej.* | 3.37 | 0.85 | 4.32 | 0.94 | 4.32 | 0.95 | | | | | 4.19 | 0.30 | 4.28 | 0.41 | 4.41 | 1.21 | 4.25 | 0.52 | 4.16 | 0.16 | | |
| 12X-6, 21–22 | 147.01 | *Para. eubej.* | 3.36 | 0.70 | | | 4.24 | 0.87 | | | | | 4.09 | 0.15 | | | | | | | | | | |
| 12X-6, 50–51 | 147.30 | *Para. eubej.* | 3.77 | 1.09 | 4.44 | 1.03 | 4.38 | 0.95 | | | | | 4.26 | 0.20 | 4.30 | 0.47 | 4.41 | 1.12 | 4.35 | 0.36 | 4.36 | 0.18 | | |
| 12X-6, 79–80 | 147.59 | *Para. eubej.* | 3.48 | 0.88 | | | 4.43 | 1.04 | | | | | 4.25 | 0.16 | | | | | | | | | | |
| 12X-6, 110–111 | 147.90 | *Para. eubej.* | 3.73 | 1.00 | 4.40 | 0.91 | 4.37 | 0.83 | | | | | 4.24 | 0.11 | 4.28 | 0.33 | | | 4.34 | 0.43 | 4.34 | 0.37 | | |
| 12X-6, 129–130 | 148.09 | *Para. eubej.* | 3.65 | 0.84 | | | 4.30 | 1.01 | | | | | 4.11 | −0.01 | | | | | | | | | | |
| 12X-CC, 10–12 | 148.20 | *Para. eubej.* | 3.37 | 0.80 | 4.29 | 1.09 | 4.25 | 1.02 | | | | | 4.05 | 0.10 | 4.05 | 0.33 | | | 4.20 | 0.30 | 4.13 | 0.25 | | |
| 13X-1, 20–22 | 149.10 | *Ps. cheniour.* | 3.10 | 0.65 | 3.84 | 0.76 | | | | | 3.71 | 0.42 | | | | | | | | | 3.74 | −0.04 | | |
| 13X-1, 60–62 | 149.50 | *Ps. cheniour.* | 2.99 | 0.62 | 3.83 | 0.78 | | | | | | | | | | | | | 3.77 | 0.23 | 3.76 | 0.00 | | |
| 13X-1, 60–62 | 149.50 | *Ps. cheniour.* | | | 3.77 | 0.78 | | | | | | | | | 3.77 | 0.78 | | | | | | | | |
| 13X-1, 97–99 | 149.87 | *Ps. cheniour.* | | | | | 3.77 | 0.76 | | | | | | | | | | | | | | | | |
| 13X-1, 140–142 | 150.30 | *Ps. cheniour.* | 2.86 | 0.50 | | | 3.54 | 0.66 | | | | | | | | | | | | | 3.60 | 0.01 | | |
| 13X-2, 20–22 | 150.60 | *Ps. cheniour.* | 2.51 | 0.25 | | | 3.32 | 0.84 | | | | | | | | | | | | | 3.34 | −0.09 | | |
| 13X-2, 60–62 | 151.00 | *Ps. cheniour.* | 2.09 | 0.35 | 3.61 | 0.74 | | | | | 3.56 | 0.67 | | | 3.72 | 0.24 | | | 3.74 | 0.35 | 3.65 | −0.04 | | |
| 13X-2, 100–102 | 151.40 | *Ps. cheniour.* | 2.62 | 0.49 | | | 3.34 | 0.65 | | | | | | | | | | | | | 3.36 | −0.13 | | |
| 13X-2, 135–137 | 151.75 | *Ps. cheniour.* | 1.70 | 0.24 | | | 3.48 | 0.69 | | | | | | | | | | | | | 2.50 | 0.08 | | |
| 13X-3, 20–22 | 152.10 | *Ps. cheniour.* | 2.42 | 0.29 | | | 2.76 | 0.55 | | | | | | | | | | | | | 2.76 | −0.07 | | |
| 13X-3, 20–22 | 152.10 | *Ps. cheniour.* | | | | | 2.78 | 0.54 | | | | | | | | | | | | | | | | |
| 13X-3, 60–62 | 152.50 | *Gl. algerian.* | 1.95 | 0.47 | | | | | 2.58 | 0.34 | 2.64 | 0.37 | | | 2.63 | −0.10 | | | 2.69 | −0.04 | 2.70 | −0.09 | | |
| 13X-3, 85–87 | 152.75 | *Gl. algerian.* | 1.67 | 0.36 | | | 2.43 | 0.94 | | | | | | | | | | | | | 2.53 | −0.21 | | |
| 13X-CC, 25–27 | 153.05 | *Gl. algerian.* | 2.08 | 0.26 | | | 2.47 | 0.55 | 2.39 | 0.40 | | | | | 2.44 | −0.07 | | | | | | | | |
| 13X-CC, 25–27 | 153.05 | *Gl. algerian.* | 1.93 | 0.36 | | | | | | | | | | | | | | | | | 2.37 | −0.26 | | |
| 13X-CC, 39–41 | 153.19 | *Gl. algerian.* | 2.23 | 0.45 | | | 2.67 | 0.41 | | | | | | | | | | | | | 2.56 | 0.03 | | |

[a]See also *Huber and Leckie* [2011b]. Planktic foraminiferal zone assignments from *Huber and Leckie* [2011a].
[b]Depth is reported in meters below seafloor (mbsf).

**Table 2.** New Albian Oxygen and Carbon Isotope Data for Bulk Carbonate and Foraminifera Obtained From ODP Hole 1049A Samples, Analyzed at the University of Missouri Stable Isotope Facility[a]

| Hole 1049C Sample | Depth[b] | Biozone | *Berthel.* spp. | | *Os. schloenb.* | | *Bolivina* sp. | | *Pleurostom.* sp. | | *Gyr. infracret.* | | *Micro. rischi*[c] | | *Mi. renilaevis*[c] | | *Ti. madecass.* | |
|---|---|---|---|---|---|---|---|---|---|---|---|---|---|---|---|---|---|---|
| | | | $\delta^{13}C$ | $\delta^{18}O$ | $\delta^{13}C$ | $\delta^{18}O$ | $\delta^{13}C$ | $\delta^{18}O$ | $\delta^{13}C$ | $\delta^{18}O$ | $\delta^{13}C$ | $\delta^{18}O$ | $\delta^{13}C$ | $\delta^{18}O$ | $\delta^{13}C$ | $\delta^{18}O$ | $\delta^{13}C$ | $\delta^{18}O$ |
| 11X-2, 124-126 | 132.44 | *T. madecass.* | | | 1.02 | 0.05 | | | | | | | 2.31 | −0.84 | 2.15 | −0.63 | | |
| 11X-2, 124-126 | 132.44 | *T. madecass.* | | | 1.00 | 0.05 | | | | | | | | | | | | |
| 11X-3, 19-21 | 132.89 | *T. madecass.* | | | 1.21 | 0.11 | | | | | | | 2.42 | −0.81 | 2.39 | −0.32 | | |
| 11X-3, 60-62 | 133.30 | *T. madecass.* | | | 1.23 | 0.10 | | | | | | | 2.51 | −0.28 | 2.50 | 0.30 | | |
| 11X-3, 100-102 | 133.70 | *T. madecass.* | | | 1.83 | 0.34 | | | | | | | 2.50 | −0.50 | 2.32 | −0.18 | | |
| 11X-4, 15-17 | 133.85 | *T. madecass.* | | | 1.53 | 0.30 | | | | | | | 2.36 | −0.27 | 2.16 | 0.01 | | |
| 11X-4, 47.5-49.5 | 134.18 | *T. madecass.* | 1.19 | 0.44 | | | | | | | | | 2.22 | −0.57 | 2.05 | −0.09 | | |
| 11X-CC, 30-31 | 134.53 | *T. madecass.* | | | 1.18 | 0.08 | | | | | | | 2.36 | −0.62 | 2.16 | −0.39 | | |
| 12X-1, 16-17 | 139.46 | *Micro. rischi* | | | 1.57 | 0.40 | | | | | | | 2.45 | −0.67 | 2.36 | −0.28 | | |
| 12X-1, 68-69 | 139.98 | *Micro. rischi* | | | 1.06 | 0.33 | | | | | | | 2.33 | −0.84 | 2.19 | −0.36 | | |
| 12X-1, 93-94 | 140.23 | *Micro. rischi* | | | 1.38 | 0.31 | | | | | | | 2.04 | −0.41 | 2.08 | −0.25 | | |
| 12X-1, 115-117 | 140.45 | *Micro. rischi* | | | 0.46 | −0.06 | | | | | | | 1.67 | −0.64 | | | | |
| 12X-1, 146-147 | 140.75 | *Micro. rischi* | | | 1.55 | 0.38 | | | | | | | 2.19 | −0.29 | 2.09 | −0.17 | | |
| 12X-2, 10-12 | 140.90 | *Micro. rischi* | | | 0.81 | 0.06 | | | | | | | | | | | | |
| 12X-2, 10-12 | 140.90 | *Micro. rischi* | | | | | | | | | | | 2.00 | −0.74 | 1.88 | −0.53 | | |
| 12X-2, 30-32 | 141.10 | *Micro. rischi* | | | 1.35 | 0.40 | | | | | 1.35 | 0.41 | 2.36 | −0.34 | 2.37 | −0.27 | 2.47 | −0.52 |
| 12X-2, 30-32 | 141.10 | *Micro. rischi* | | | 1.39 | 0.43 | | | | | | | | | | | | |
| 12X-2, 76-78 | 141.56 | *Micro. rischi* | | | 0.93 | 0.18 | | | | | | | | | | | 2.22 | −1.27 |
| 12X-2, 76-78 | 141.56 | *Micro. rischi* | | | 0.81 | 0.15 | | | | | | | | | | | | |
| 12X-2, 89-91 | 141.69 | *Micro. rischi* | | | 0.72 | 0.21 | | | | | | | 1.78 | −1.16 | | | | |
| 12X-2, 94-96 | 141.74 | *Micro. rischi* | | | | | | | | | 1.60 | 0.44 | | | | | | |
| 12X-2, 97-99 | 141.77 | *Micro. rischi* | | | | | | | | | 1.41 | 0.42 | | | | | | |
| 12X-2, 112-114 | 141.92 | *Micro. rischi* | | | 1.05 | 0.38 | | | | | | | | | | | | |
| 12X-2, 112-114 | 141.92 | *Micro. rischi* | | | 1.21 | 0.43 | | | | | | | | | | | | |
| 12X-2, 116 | 141.96 | *Micro. rischi* | | | | | | | | | 1.93 | 0.40 | | | | | | |
| 12X-2, 121-123 | 142.01 | *Micro. rischi* | | | 1.07 | 0.29 | | | | | | | | | | | | |
| 12X-3, 13-14 | 142.43 | *Micro. rischi* | | | 1.19 | 0.26 | | | | | | | | | | | | |
| 12X-3, 29.5 | 142.59 | *Micro. rischi* | 1.35 | 0.41 | | | | | | | | | | | | | | |
| 12X-3,, 39-41 | 142.69 | *Micro. rischi* | | | 1.53 | 0.37 | | | 1.83 | 0.94 | | | | | | | | |
| 12X-3, 67-69 | 142.97 | *Micro. rischi* | | | | | | | 1.50 | 0.43 | | | | | | | | |
| 12X-3, 81-83 | 143.11 | *Micro. rischi* | | | | | 0.85 | 0.02 | | | | | | | | | | |
| 12X-3, 84-86 | 143.14 | *Micro. rischi* | | | | | 0.99 | −0.01 | | | | | | | | | | |
| 12X-3, 116 | 143.46 | *Micro. rischi* | | | 1.93 | 0.40 | | | | | | | | | | | | |
| 12X-4, 30-32 | 144.11 | *Micro. rischi* | 1.95 | 0.46 | | | | | | | | | 2.13 | −1.07 | 2.40 | −0.07 | | |
| 12X-4, 57-59 | 144.36 | *Micro. rischi* | | | 1.45 | 0.43 | | | | | | | | | | | | |
| 12X-4,70-72 | 144.49 | *Micro. rischi* | | | 1.39 | 0.36 | | | | | | | | | 1.64 | −0.93 | | |
| 12X-4,89-91 | 144.68 | *Micro. rischi* | | | | | | | | | | | | | | | | |
| 12X-4, 92-94 | 144.71 | *Micro. rischi* | | | 1.05 | 0.24 | | | | | | | 2.74 | −0.69 | 2.53 | −0.84 | | |
| 12X-4, 130-132 | 145.11 | *Micro. rischi* | 0.88 | 0.52 | | | | | | | | | 2.52 | 0.36 | 2.28 | 0.46 | | |
| 12X-4, 140-142 | 145.21 | *Micro. rischi* | | | | | | | | | | | 2.51 | 0.66 | 2.35 | 0.65 | | |
| 12X-4, 140-142 | 145.21 | *Micro. rischi* | 0.92 | 0.46 | | | | | | | | | 2.57 | 0.74 | | | | |

[a]Planktic foraminiferal zone assignments from *Huber and Leckie* [2011a].
[b]Depth is reported in meters below seafloor (mbsf).
[c]*H. speetonensis* and *H.* aff. *H. trocoidea* of *Erbacher et al.* [2001] are the same as *Mi. renilaevis* and *Mi. rischi*, respectively, of this study.

**Table 3.** New Aptian and Albian Oxygen and Carbon Isotope Data for Bulk Carbonate and Foraminifera Samples Obtained From ODP Hole 1049C, Analyzed at Royal Holloway University[a]

| Hole 1049C Sample | Biozone | Depth[b] (mbsf) | Bulk Carbonate | | *Gyr. infracret.* | | *Pa. eubejou.* | |
|---|---|---|---|---|---|---|---|---|
| | | | $\delta^{13}C$ | $\delta^{18}O$ | $\delta^{13}C$ | $\delta^{18}O$ | $\delta^{13}C$ | $\delta^{18}O$ |
| 12X-1, 0–1 | *Micro. rischi* | 139.30 | 1.48 | −0.97 | | | | |
| 12X-1, 10–11 | *Micro. rischi* | 139.40 | 1.98 | −1.05 | | | | |
| 12X-1, 20–21 | *Micro. rischi* | 139.50 | 2.03 | −0.71 | | | | |
| 12X-1, 30–31 | *Micro. rischi* | 139.60 | 2.11 | −0.68 | | | | |
| 12X-1, 40–41 | *Micro. rischi* | 139.70 | 2.35 | −0.18 | | | | |
| 12X-1, 50–51 | *Micro. rischi* | 139.80 | 1.95 | −0.49 | | | | |
| 12X-1, 60–61 | *Micro. rischi* | 139.90 | 2.11 | −0.71 | | | | |
| 12X-1, 70–71 | *Micro. rischi* | 140.00 | 2.00 | −0.84 | | | | |
| 12X-1, 80–81 | *Micro. rischi* | 140.10 | 2.24 | −0.63 | | | | |
| 12X-1, 90–91 | *Micro. rischi* | 140.20 | 2.03 | −0.49 | | | | |
| 12X-1, 100–101 | *Micro. rischi* | 140.30 | 1.74 | −0.68 | | | | |
| 12X-1, 110–111 | *Micro. rischi* | 140.40 | 1.71 | −0.50 | | | | |
| 12X-1, 120–121 | *Micro. rischi* | 140.50 | 1.57 | −1.00 | | | | |
| 12X-1, 130–131 | *Micro. rischi* | 140.60 | 1.93 | −1.34 | | | | |
| 12X-1, 140–141 | *Micro. rischi* | 140.70 | 2.03 | −0.66 | | | | |
| 12X-2, 0–1 M | *Micro. rischi* | 140.80 | 2.06 | −0.71 | | | | |
| 12X-2, 10–11 | *Micro. rischi* | 140.90 | 1.70 | −0.69 | | | | |
| 12X-2, 19–20 | *Micro. rischi* | 140.99 | 1.12 | −1.61 | | | | |
| 12X-2, 30–31 | *Micro. rischi* | 141.10 | 1.74 | −1.11 | | | | |
| 12X-2, 40–41 | *Micro. rischi* | 141.20 | 2.07 | −0.74 | | | | |
| 12X-2, 50–51 | *Micro. rischi* | 141.30 | 2.28 | −0.32 | | | | |
| 12X-2, 60–61 | *Micro. rischi* | 141.40 | 2.06 | −0.83 | | | | |
| 12X-2, 70–71 | *Micro. rischi* | 141.50 | 2.25 | −0.66 | | | | |
| 12X-2, 81–82 | *Micro. rischi* | 141.61 | 1.79 | −1.11 | | | | |
| 12X-2, 90–91 | *Micro. rischi* | 141.70 | 1.17 | −1.70 | | | | |
| 12X-2, 100–101 | *Micro. rischi* | 141.80 | 1.07 | −2.45 | | | | |
| 12X-2, 111–112 | *Micro. rischi* | 141.91 | 1.87 | −2.16 | | | | |
| 12X-2, 120–121 | *Micro. rischi* | 142.00 | 1.81 | −1.36 | | | | |
| 12X-2, 131–132 | *Micro. rischi* | 142.11 | 1.91 | −1.20 | | | | |
| 12X-2, 140–141 | *Micro. rischi* | 142.20 | 1.89 | −1.13 | | | | |
| 12X-3, 0–1 | *Micro. rischi* | 142.30 | 1.86 | −1.14 | | | | |
| 12X-3, 10–11 | *Micro. rischi* | 142.40 | 1.86 | −1.30 | 0.66 | −1.60 | | |
| 12X-3, 20–21 | *Micro. rischi* | 142.50 | 1.33 | −0.95 | | | | |
| 12X-3, 30–31 | *Micro. rischi* | 142.60 | 1.67 | −1.80 | | | | |
| 12X-3, 40–41 | *Micro. rischi* | 142.70 | 2.11 | −1.75 | | | | |
| 12X-3, 42–43 | *Micro. rischi* | 142.72 | 1.96 | −1.90 | | | | |
| 12X-3, 88.5–89 | *Micro. rischi* | 143.18 | 2.54 | −1.28 | 1.80 | 0.19 | | |
| 12X-3, 90–91 | *Micro. rischi* | 143.20 | 2.74 | −0.56 | 1.12 | −1.57 | | |
| 12X-3, 100–101 | *Micro. rischi* | 143.30 | 2.26 | −0.58 | 1.21 | −1.14 | | |
| 12X-3, 110–111 | *Micro. rischi* | 143.40 | 2.13 | −0.15 | | | | |
| 12X-3, 120–121 | *Micro. rischi* | 143.50 | 2.23 | −0.35 | | | | |
| 12X-3, 130–131 | *Micro. rischi* | 143.60 | 2.42 | −0.34 | | | | |
| 12X-3, 140–141 | *Micro. rischi* | 143.70 | 2.59 | −0.40 | | | | |
| 12X-4, 0–1 | *Micro. rischi* | 143.80 | 2.18 | −0.41 | | | | |
| 12X-4, 10–11 | *Micro. rischi* | 143.90 | 2.49 | 0.04 | | | | |
| 12X-4, 19–20 | *Micro. rischi* | 143.99 | 2.49 | −0.73 | | | | |
| 12X-4, 30–31 | *Micro. rischi* | 144.10 | 2.27 | −0.73 | | | | |
| 12X-4, 40–41 | *Micro. rischi* | 144.20 | 2.02 | −0.34 | | | | |
| 12X-4, 50–51 | *Micro. rischi* | 144.30 | 2.30 | 0.02 | | | | |
| 12X-4, 60–61 | *Micro. rischi* | 144.40 | 1.93 | −0.63 | | | | |
| 12X-4, 70–71 | *Micro. rischi* | 144.50 | 2.09 | −1.20 | | | | |
| 12X-4, 80–81 | *Micro. rischi* | 144.60 | 2.23 | −0.56 | | | | |
| 12X-4, 90–91 | *Micro. rischi* | 144.70 | 1.88 | −0.68 | | | | |
| 12X-4, 100–101 | *Micro. rischi* | 144.80 | 1.63 | −1.27 | | | | |
| 12X-4, 110–111 | *Micro. rischi* | 144.90 | 1.87 | −0.19 | | | | |
| 12X-4, 120–121 | *Micro. rischi* | 145.00 | 1.68 | −1.19 | | | | |
| 12X-4, 130–131 | *Micro. rischi* | 145.10 | 1.98 | −0.14 | | | | |
| 12X-4, 131–132 | *Micro. rischi* | 145.11 | 1.67 | −0.25 | | | | |
| 12X-4, 132–133 | *Micro. rischi* | 145.12 | 1.77 | −0.43 | | | | |
| 12X-4, 133–134 | *Micro. rischi* | 145.13 | 1.86 | −0.60 | | | | |
| 12X-4, 134–135 | *Micro. rischi* | 145.14 | 1.31 | −0.66 | | | | |
| 12X-4, 135–136 | *Micro. rischi* | 145.15 | 1.68 | −0.92 | | | | |

**Table 3.** (continued)

| Hole 1049C Sample | Biozone | Depth[b] (mbsf) | Bulk Carbonate | | *Gyr. infracret.* | | *Pa. eubejou.* | |
|---|---|---|---|---|---|---|---|---|
| | | | $\delta^{13}C$ | $\delta^{18}O$ | $\delta^{13}C$ | $\delta^{18}O$ | $\delta^{13}C$ | $\delta^{18}O$ |
| 12X-4, 136–137 | *Micro. rischi* | 145.16 | 1.46 | −0.63 | | | | |
| 12X-4, 137–138 | *Micro. rischi* | 145.17 | 1.75 | −0.35 | | | | |
| 12X-4, 138–139 | *Micro. rischi* | 145.18 | 1.87 | −0.27 | | | | |
| 12X-4, 139–140 | *Micro. rischi* | 145.19 | 1.87 | −0.13 | | | | |
| 12X-4, 140–141 | *Micro. rischi* | 145.20 | 1.80 | −0.43 | | | | |
| 12X-4, 141–142 | *Micro. rischi* | 145.21 | 1.78 | −0.53 | | | | |
| 12X-4, 142–143 | *Micro. rischi* | 145.22 | 1.78 | −0.30 | 1.14 | 0.09 | 3.35 | −0.53 |
| 12X-4, 143–144 | *Micro. rischi* | 145.23 | 1.75 | −0.73 | 1.21 | −0.15 | 3.46 | −0.28 |
| 12X-4, 144–145 | *Micro. rischi* | 145.24 | 1.79 | −0.71 | 1.12 | −0.12 | 2.80 | −0.17 |
| 12X-4, 145–146 | *Micro. rischi* | 145.25 | 1.73 | −0.74 | 1.12 | −0.34 | 2.55 | −0.47 |
| 12X-4, 146–147 | *Micro. rischi* | 145.26 | 1.96 | −0.98 | 1.09 | −0.37 | 2.51 | −1.00 |
| 12X-4, 147–148 | *Micro. rischi* | 145.27 | 2.07 | −0.34 | 1.27 | −0.26 | 2.52 | −1.02 |
| 12X-4, 148–149 | *Micro. rischi* | 145.28 | 2.56 | −0.46 | 1.61 | −0.31 | 2.46 | −0.95 |
| 12X-4, 149–150 | *Para. eubej.* | 145.29 | 3.78 | 0.10 | 2.50 | 0.06 | 3.22 | −0.91 |
| 12X-5, 0–1 | *Para. eubej.* | 145.30 | 3.51 | 0.12 | 2.95 | 0.44 | 3.65 | −0.26 |
| 12X-5, 1–2 | *Para. eubej.* | 145.31 | 3.16 | −0.49 | 2.60 | 0.18 | 3.41 | −0.24 |
| 12X-5, 2–3 | *Para. eubej.* | 145.32 | 3.18 | −0.21 | 2.91 | 0.44 | 3.51 | −0.10 |
| 12X-5, 3–4 | *Para. eubej.* | 145.33 | 3.52 | −0.04 | 3.24 | 0.56 | 3.63 | −0.31 |
| 12X-5, 4–5 | *Para. eubej.* | 145.34 | 3.61 | −0.07 | 2.83 | 0.39 | 3.77 | −0.04 |
| 12X-5, 5–6 | *Para. eubej.* | 145.35 | 3.78 | 0.06 | | | | |
| 12X-5, 6–7 | *Para. eubej.* | 145.36 | 3.86 | 0.18 | | | | |
| 12X-5, 7–8 | *Para. eubej.* | 145.37 | 3.80 | 0.40 | | | | |
| 12X-5, 8–9 | *Para. eubej.* | 145.38 | 3.87 | 0.33 | | | | |
| 12X-5, 9–10 | *Para. eubej.* | 145.39 | 3.60 | −0.09 | | | | |
| 12X-5, 10–11 | *Para. eubej.* | 145.40 | 3.48 | −0.02 | 2.76 | 0.10 | 3.64 | −0.39 |
| 12X-5, 11–12 | *Para. eubej.* | 145.41 | 3.46 | 0.14 | | | | |
| 12X-5, 12–13 | *Para. eubej.* | 145.42 | 3.60 | 0.19 | | | | |
| 12X-5, 13–14 | *Para. eubej.* | 145.43 | 3.63 | 0.12 | | | | |
| 12X-5, 14–15 | *Para. eubej.* | 145.44 | 3.47 | 0.16 | | | | |
| 12X-5, 15–16 | *Para. eubej.* | 145.45 | 3.62 | 0.37 | | | | |
| 12X-5, 16–17 | *Para. eubej.* | 145.46 | 3.46 | −0.03 | | | | |
| 12X-5, 17–18 | *Para. eubej.* | 145.47 | 3.34 | 0.02 | | | | |
| 12X-5, 18–19 | *Para. eubej.* | 145.48 | 3.35 | −0.09 | | | | |
| 12X-5, 19–20 | *Para. eubej.* | 145.49 | 3.33 | 0.03 | 2.80 | 0.15 | 3.86 | −0.25 |
| 12X-5, 20–21 | *Para. eubej.* | 145.50 | 3.29 | 0.06 | | | | |
| 12X-5, 21–22 | *Para. eubej.* | 145.51 | 3.49 | 0.36 | | | | |
| 12X-5, 29–30 | *Para. eubej.* | 145.59 | 3.50 | 0.43 | 2.78 | 0.01 | 3.78 | −0.10 |
| 12X-5, 39–40 | *Para. eubej.* | 145.69 | 3.37 | −0.27 | 2.39 | −0.28 | 3.45 | −0.38 |
| 12X-5, 50–51 | *Para. eubej.* | 145.80 | 3.75 | 0.31 | 3.24 | 0.62 | 3.66 | −0.44 |
| 12X-5, 59–60 | *Para. eubej.* | 145.89 | 3.94 | 0.44 | 2.71 | −0.24 | 3.41 | −0.94 |
| 12X-5, 69–70 | *Para. eubej.* | 145.99 | 3.50 | 0.03 | 2.73 | 0.04 | 3.76 | −0.67 |
| 12X-5, 80–81 | *Para. eubej.* | 146.10 | 3.60 | 0.06 | 2.15 | −0.88 | 3.89 | −0.59 |
| 12X-5, 99–100 | *Para. eubej.* | 146.29 | 4.05 | 0.63 | | | 3.40 | −1.10 |
| 12X-5, 109–110 | *Para. eubej.* | 146.39 | 3.65 | −0.03 | 2.71 | 0.21 | 3.69 | −0.45 |
| 12X-5, 121–122 | *Para. eubej.* | 146.51 | 3.78 | 0.49 | 3.23 | −0.06 | 4.11 | 0.26 |
| 12X-5, 130–131 | *Para. eubej.* | 146.60 | 4.06 | 0.43 | 3.30 | 0.10 | 4.08 | −0.23 |
| 12X-5, 139–140 | *Para. eubej.* | 146.69 | 4.00 | 0.26 | 3.41 | 0.34 | 4.18 | −0.17 |
| 12X-6, 0–1 | *Para. eubej.* | 146.80 | 3.90 | −0.01 | 2.67 | −0.41 | 4.25 | 0.38 |
| 12X-6, 10–11 | *Para. eubej.* | 146.90 | 3.89 | 0.46 | | | 3.81 | −0.67 |
| 12X-6, 21–22 | *Para. eubej.* | 147.01 | 4.15 | 0.34 | 2.94 | −0.17 | 4.17 | 0.03 |
| 12X-6, 30–31 | *Para. eubej.* | 147.10 | 3.92 | 0.30 | 3.01 | −0.01 | 4.08 | −0.23 |
| 12X-6, 40–41 | *Para. eubej.* | 147.20 | 4.24 | 0.53 | | | 4.13 | −0.30 |
| 12X-6, 50–51 | *Para. eubej.* | 147.30 | 4.07 | 0.07 | 3.04 | 0.08 | 4.41 | 0.33 |
| 12X-6, 60–61 | *Para. eubej.* | 147.40 | 4.19 | 0.26 | 3.12 | 0.37 | 4.20 | 0.08 |
| 12X-6, 70–71 | *Para. eubej.* | 147.50 | 4.24 | 0.82 | 3.24 | 0.70 | 4.28 | 0.04 |
| 12X-6, 79–80 | *Para. eubej.* | 147.59 | 4.14 | 0.53 | 2.67 | −0.51 | 4.26 | 0.02 |
| 12X-6, 90–91 | *Para. eubej.* | 147.70 | 4.17 | 0.61 | 2.47 | −0.81 | 4.14 | 0.01 |
| 12X-6, 100–101 | *Para. eubej.* | 147.80 | 4.30 | 0.64 | 2.74 | 0.15 | 4.24 | 0.23 |
| 12X-6, 110–111 | *Para. eubej.* | 147.90 | 4.24 | 0.40 | | | 4.11 | −0.25 |
| 12X-6, 120–121 | *Para. eubej.* | 148.00 | 4.14 | 0.36 | | | 4.17 | 0.13 |
| 12X-6, 129–130 | *Para. eubej.* | 148.09 | | | 2.53 | −0.30 | 4.26 | −0.14 |

[a]Planktic foraminiferal zone assignments from *Huber and Leckie* [2011a].
[b]Depth is reported in meters below seafloor (mbsf).

**Table 4.** New Oxygen and Carbon Isotope Data for Foraminifera Across the Aptian/Albian Boundary of ODP Hole 1049A, Analyzed at the University of Missouri Stable Isotope Facility[a]

| Hole 1049A Samples | Depth[b] (mbsf) | Biozone | *Berth.* sp. | | *Os. schloen.* | | *Gy. infracret.* | | *Par. eubej.* | | *Par. trans.* | | *Hd. infracr.* | | *Mi. rischi* | | *Mi. renilaevis* | | *Pg. blakeno.* | | *Hd. aptiana* | |
|---|---|---|---|---|---|---|---|---|---|---|---|---|---|---|---|---|---|---|---|---|---|---|
| | | | $\delta^{13}C$ | $\delta^{18}O$ | $\delta^{13}C$ | $\delta^{18}O$ | $\delta^{13}C$ | $\delta^{18}O$ | $\delta^{13}C$ | $\delta^{18}O$ | $\delta^{13}C$ | $\delta^{18}O$ | $\delta^{13}C$ | $\delta^{18}O$ | $\delta^{13}C$ | $\delta^{18}O$ | $\delta^{13}C$ | $\delta^{18}O$ | $\delta^{13}C$ | $\delta^{18}O$ | $\delta^{13}C$ | $\delta^{18}O$ |
| 20X-4, 43–45 cm | 158.43 | *Micro. rischi* | | | 1.00 | 0.50 | 1.13 | 0.80 | 3.31 | −0.38 | | | | | 2.35 | −0.01 | 2.19 | 0.04 | | | | |
| 20X-4, 45–50 cm | 158.45 | *Micro. rischi* | | | 1.02 | 0.54 | 1.14 | 0.74 | 3.00 | −0.44 | 4.09 | −0.15 | | | 2.31 | 0.05 | 1.97 | −0.03 | | | | |
| 20X-4, 45–50 cm | 158.45 | *Micro. rischi* | | | | | | | 3.70 | −0.03 | | | | | | | | | | | | |
| 20X-4, 53–55 cm | 158.53 | *Para. eubej.* | 1.35 | 0.42 | 1.27 | 0.43 | 1.07 | 0.38 | 2.77 | −0.53 | | | | | 2.31 | −0.21 | 2.14 | −0.23 | 3.56 | 0.77 | | |
| 20X-4, 53–55 cm | 158.53 | *Para. eubej.* | 1.29 | 0.47 | | | | | 2.80 | −0.37 | | | | | | | | | | | | |
| 20X-4, 59–61 cm | 158.59 | *Para. eubej.* | | | 3.68 | 0.83 | 2.95 | 0.58 | 3.58 | −0.08 | 4.34 | 0.13 | 3.90 | 0.35 | | | 2.27 | −0.07 | 4.09 | 0.98 | 3.31 | 0.15 |
| 20X-4, 59–61 cm | 158.59 | *Para. eubej.* | | | 3.54 | 0.81 | | | | | | | 3.91 | 0.40 | | | | | | | | |

[a]Planktic foraminiferal zone assignments from *Huber and Leckie* [2011a].
[b]Depth is reported in meters below seafloor (mbsf).

[13] Additional stable isotope data from lower Albian samples of Hole 1049C that are discussed in this study were published by *Erbacher et al.* [2001] and *Huber and Leckie* [2011b]. Paleotemperature estimates for benthic and planktic foraminifera are based on equation 1 of *Bemis et al.* [1998] with the assumption that mean seawater $\delta^{18}O$ value was $-1‰_{SMOW}$ (which corresponds to a value of −1.27‰ for the $\delta^{18}O$ of water in the temperature equation) for an ice-free Earth [*Shackleton and Kennett*, 1975].

### 3.3. Strontium Isotope Analyses

[14] $^{87}Sr/^{86}Sr$ ratios were measured on bulk sediment and mixed foraminiferal separates (∼50–100 individuals/analysis) spanning the study interval. Picked separates were ultrasonically cleaned and examined under a binocular microscope. The taxonomic composition of the separates was not considered and both the species present and their relative abundances varied among samples. As above, analyses were performed at several labs. Mixed separates were run at the University of North Carolina, Royal Holloway University, and Oxford University. At the University of North Carolina, foraminiferal separates were dissolved in 1.7 M acetic acid, processed using EiChrom Sr Spec resin, and analyzed on a VG Sector 54 thermal ionization mass spectrometer. External precision is estimated at ±0.000 010 (1 SE). At Royal Holloway and Oxford University, between 3 and 25 mg of the bulk sediment fraction >0.150 mm was weighed into centrifuge tubes and digested with 10% acetic acid. Acid was being added as long as the carbonate in the sample reacted but care was taken to assure that a small amount of solid residue remained. This was to minimize contamination by Sr from non-biogenic components in the sediment. Strontium was separated by standard ion exchange chemistry using Sr Spec resin. Measurements were made with a VG 354 thermal ionization mass spectrometer. Individual values are reported with 2 SE. External precision based on repeated measurement of the standard was estimated at ±0.000 018 (2 SE). Results reported for each lab were normalized to a value of 0.710250 for NIST 987.

## 4. Stable Isotopic Results

### 4.1. Foraminiferal Preservation

[15] Early Albian foraminifera from Blake Nose are remarkably well preserved. Nearly all samples contain specimens that are translucent under the stereomicroscope and appear to be 'glassy' (sensu *Pearson et al.* [2001]; Figure 3a). When viewed at high magnification with an SEM, these specimens show no evidence of shell recrystallization or chamber infilling (Figure 3b). Most Late Aptian shells are not as well preserved. They are opaque and white under the light microscope and have a 'frosty' appearance (sensu *Sexton et al.* [2006]; Figure 3c). SEM images show some degree of shell recrystallization with the most strongly altered specimens exhibiting neomorphic calcite crystals on the inner chamber walls, complete obliteration of the original bilamellar wall, and infilling of the wall pores in SEM images (Figure 3d). None of the Aptian shells are infilled by secondary calcite.

### 4.2. Oxygen Isotopes

[16] Late Aptian benthic $\delta^{18}O$ values, as generalized from results for *Berthelina* spp., vary from 0.5 to 0.2‰ within the

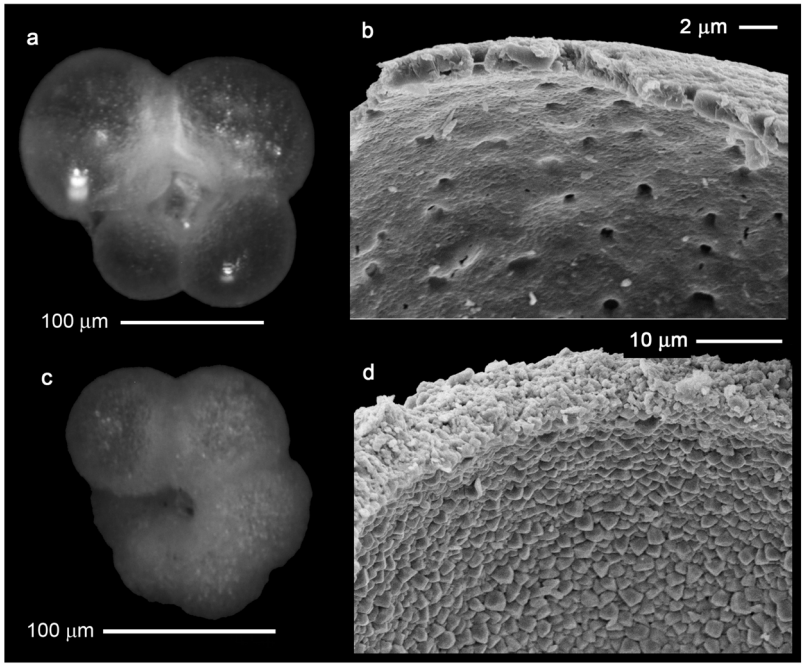


**Figure 3.** Shell preservation of planktic foraminifera across the Aptian/Albian boundary of ODP Hole 1049 C. (a) Composite focused stereomicroscope image showing 'glassy' (=optically translucent) appearance of early Albian *Microhedbergella renilaevis* (Sample 1049 C-12X-3, 39–41 cm); (b) SEM of chamber interior for 'glassy' *Microhedbergella renilaevis* showing no evidence of pore infilling, shell recyrstallization or secondary precipitation of calcite (Sample 1049 C-12X-3, 39–41 cm); (c) stereomicroscope image of 'frosty' *Hedbergella infracretacea* showing moderately good shell preservation; and (d) SEM of chamber interior for 'frosty' *Hedbergella infracretacea* showing neomorphic growth of calcite crystals and fine-scale wall recrystallization that has obliterated original shell microlayering and closure of wall pores (Sample 1049 C-12X-3, 39–41 cm).

*Gl. algerianus-Hd. trocoidea* Zones, increase to a maximum of 1.1‰ in the *Pa. eubejaouaensis* Zone and then decrease to 0.5‰ just below the Aptian/Albian contact. Bulk carbonate $\delta^{18}$O values generally parallel this trend, but the difference between bulk and benthic values increases up-section. In the oldest samples bulk values are the same or higher than co-occurring benthic foraminifer $\delta^{18}$O values whereas higher in the study interval they plot between benthic and planktic values (Figures 4 and 5 and Tables 1–4). A similar trend is apparent in analyses of planktic foraminifera. In late Aptian samples, five species (*Globigerinelloides algerianus, Gl. aptiensis*, *Gl.ferreolensis*, *Pseudoguembelitria blakenosensis*, and *Hedbergella aptiana*) have $\delta^{18}$O values similar to or higher than corresponding benthic values and two species (*Hd. trocoidea* and *Pa. eubejaouaensis*) have consistently lower values than benthic values. The lowest Aptian planktic $\delta^{18}$O values were measured on separates of *Pa. eubejaouaensis* and reach minimum values near −1.0‰, approximately 1.5 m below the Aptian/Albian boundary.

[17] Across the Aptian/Albian boundary contact bulk carbonate $\delta^{18}$O ratios show a sharp decrease by almost 0.9‰ while benthic foraminifera decrease by almost 0.5‰. In the lower Albian *Mi. rischi* Zone, benthic foraminifera show relatively constant values varying between 0.5 and −0.2‰. Early Albian bulk carbonate $\delta^{18}$O values are close to or lower than corresponding values from the planktic species *Microhedbergella rischi* and *Mi. renilaevis*, which generally range between −0.3 and −0.8‰. A 1‰ decrease in the $\delta^{18}$O of bulk carbonate and the microhedbergellids in the lowermost 1.67 m of the Albian is followed by an additional decrease to −2.3‰ within the OAE 1b black shale interval and bulk carbonate reaches even lower values (−2.5‰) within 1 m above the black shale. Planktic foraminifer values generally vary between 0.0 and −0.8‰ for the remainder of the lower Albian section, while the bulk carbonate yields slightly lower values. Offset between the species of *Microhedbergella* is remarkably consistent, with *Mi. renilaevis* plotting 0.1 to 0.5‰ higher than *Mi. rischi* [see *Huber and Leckie*, 2011a, Figure 19].

### 4.3. Carbon Isotopes

[18] Carbon isotope records for bulk carbonate, benthic foraminifera, and planktic foraminifera show consistent interspecies offsets and parallel trends for most of the upper Aptian-lower Albian record (Figures 4 and 5 and Tables 1–4). In the upper Aptian, $\delta^{13}$C values for bulk carbonate and planktic foraminifera are nearly the same. These values increase from 2.4‰ in the *Globigerinelloides algerianus* Zone to 4.4‰ in the middle *Paraticinella eubejaouaensis* Zone and decrease to 3.8‰ just below Aptian/Albian contact. Throughout the Aptian interval, benthic foraminifer $\delta^{13}$C values are 0.4 to 0.7‰ lower than the bulk carbonate and planktic foraminifer values.

[19] Benthic and bulk carbonate $\delta^{13}$C values show a 1.5‰ and 2.2‰ negative shift, respectively, across the Aptian/Albian boundary, with benthic values reaching a minimum of

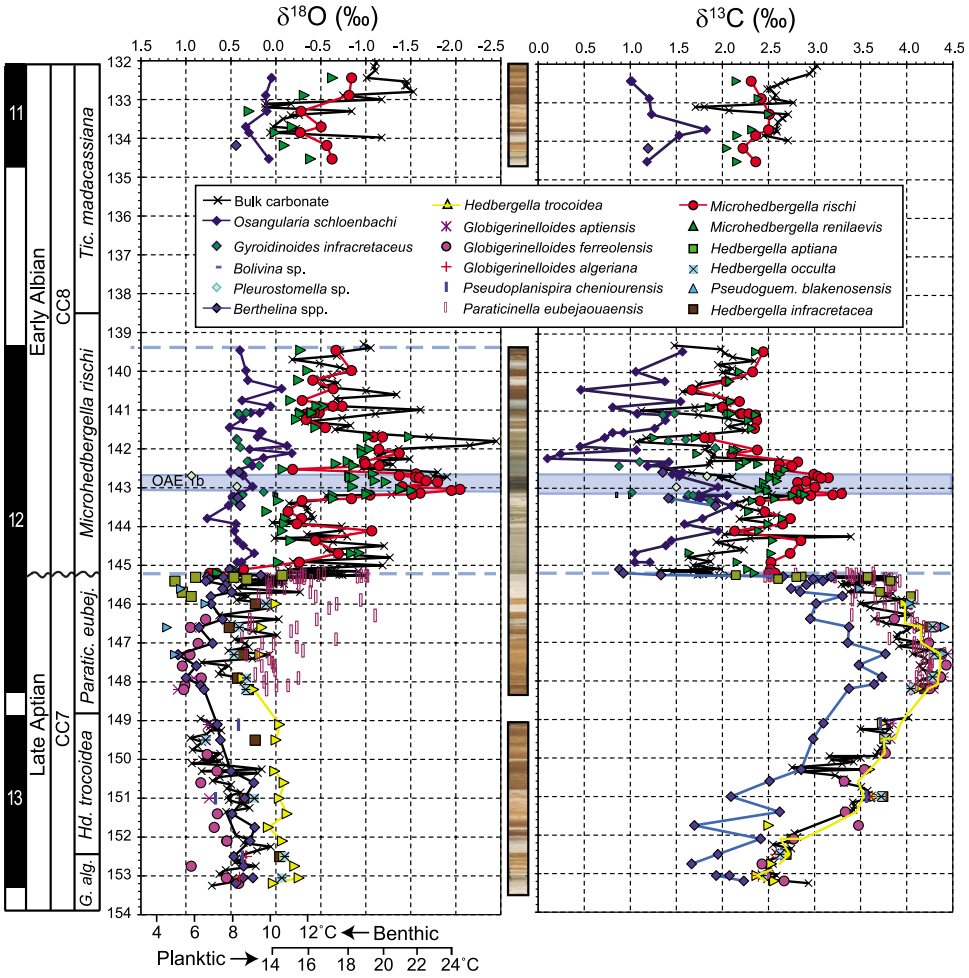


**Figure 4.** Oxygen and carbon isotope ratios from single taxon planktic and benthic foraminifera samples and bulk carbonate samples from the upper Aptian-lower Albian of ODP Hole 1049C plotted with composite images of the drill cores. All species listed in the left column of the legend are benthic foraminifera, whereas the middle and right columns list planktic species. Data points for several benthic and planktic species are connected by two-point running average curves and the bulk carbonate data are connected by a 3-point running average curve. Columns to the left of the plots represent (left to right) core recovery (black = interval of recovered core), age, calcareous nannofossil biozone (from *Browning and Watkins* [2008]), planktic foraminifer biozones (from *Huber and Leckie* [2011a]) and core depths (in meters below seafloor). The horizontal blue shading represents the interval comprising the OAE 1b black shale reported by *Erbacher et al.* [2001] and the blue horizontal dashed line marks the level of the Aptian/Albian boundary unconformity. Paleotemperature scales at the bottom of the oxygen isotope graph are calculated using the equation 1 of *Bemis et al.* [1998] with the assumption that mean seawater $\delta^{18}O$ value was $-1‰_{SMOW}$ for an ice-free Earth [*Shackleton and Kennett*, 1975] and a salinity correction for planktic species using the salinity correction of *Zachos et al.* [1994] for 25°N. Isotope data presented in Tables 2–4, by *Erbacher et al.* [2001], and by *Huber and Leckie* [2011a, 2011b].

0.9‰ 17 cm above the boundary level (145.11 mbsf). Benthic values increase to about 2‰ at 1.65 m above the boundary (143.63 mbsf), decrease to a minimum of 0.1‰ at in the middle *Mi. rischi* Zone (142.23 mbsf) and range between 0.5 and 1.6‰ in the upper part of the lower Albian section.

[20] Early Albian $\delta^{13}C$ values from the two planktic species analyzed show remarkable consistency, with *Mi. rischi* plotting 0.2 to 0.6‰ higher than co-occurring *Mi. renilaevis*. *Microhedbergella rischi* $\delta^{13}C$ values gradually increase from 2.5 to 3.3‰ from just above the Aptian/Albian contact to within the black shale bed (143.14 mbsf) and then fluctuate between 1.7 and 2.5‰ in the remaining Albian samples. Bulk carbonate $\delta^{13}C$ values parallel those of the planktic species but are generally 0.5 to 1.0‰ lower. An exception to this is within 0.3 m above the black shale bed where the bulk values are as low as corresponding benthic values.

### 4.4. Strontium Isotopic Results

[21] Results for the mixed separates show a large (~0.000 200) increase across a <10 cm interval (Table 5). In samples run at the University of North Carolina and at Royal

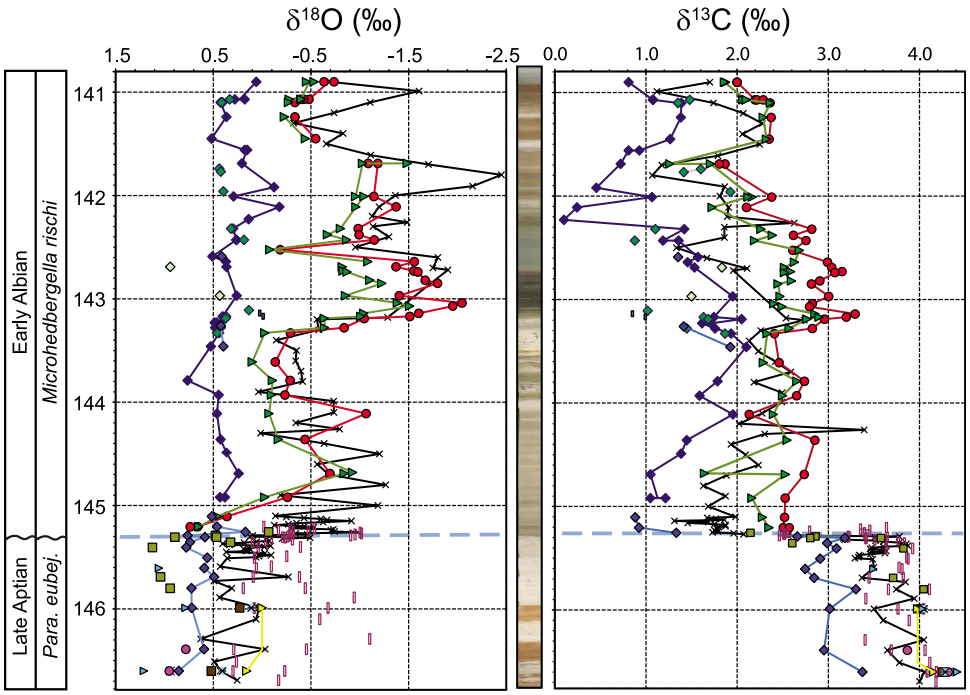


**Figure 5.** Oxygen and carbon isotope graphs across the Aptian/Albian boundary of ODP Hole 1049C from between 140.80 and 146.8 m below sea floor plotted relative to composited core images showing the sharp lithologic contact between the upper Aptian white clay-rich chalk to the overlying lower Albian gray calcareous claystone. See Figure 4 caption for key to symbols and sources of isotope data.

Holloway University, the values agree closely both based on stratigraphic trends and for replicates from the same samples. For samples run at the University of Oxford, on the other hand, stratigraphic trends are identical, but measured values are consistently ~0.000 030 higher than values from the other two labs. Similar offsets have been previously demonstrated [*MacLeod et al.*, 2001, 2003] but this is the first time this inter-lab offset has been shown in replicates from the same samples as well as in trends across the same interval. Despite this more direct comparison, we still have no good explanation for the offset. To facilitate subsequent comparison to the Cretaceous seawater curve [*McArthur and Howarth*, 2004], values not run at Oxford were increased by 0.000 030. With this correction, upper Aptian ratios vary between a narrow range 0.707224 and 0.707240, and then abruptly, but smoothly, increase to 0.707448 approximately 10 cm above the Aptian/Albian boundary (145.26 mbsf). Lower Albian ratios vary between 0.707379 and 0.707414 (Figure 7).

## 5. Discussion

### 5.1. Aptian/Albian Boundary Unconformity at Site 1049

[22] The presence of an unconformity at the Aptian/Albian boundary of Site 1049 is indicated by the coincidence of abrupt and substantial changes in the planktic foraminiferal assemblages, major geochemical shifts and a sharp lithologic contact separating a late Aptian clay-rich marl and an early Albian pelagic chalk (Figures 1 and 4–7). The negative shifts in $\delta^{13}C$ and $\delta^{18}O$ recorded in benthic foraminifera and bulk carbonate accompanied by the positive shift in $^{87}Sr/^{86}Sr$ isotope ratios at this boundary level are too large and abrupt to be explained by any known tectonic, climatic or

**Table 5.** Age Model Using Planktic Foraminifer (F) and Calcareous Nannofossil (N) Datum Ages From the Geologic Timescale of *Gradstein et al.* [2004]

| Datum Type | Datum Event | Plot Code | Young Age | Top Depth[a] | Bottom Depth[a] |
|---|---|---|---|---|---|
| F | FAD *Ticinella madecassiana*[b] | tTm | 109.50 | 138.34 | 138.78 |
| N | FAD *Hayesites albiensis*[c] | bHa | 111.69 | 145.00 | 145.22 |
| N | FAD *Praediscosphaera columnata* s.s.[c] | bPc | 112.02 | 145.26 | 145.29 |
| F | LAD *Paraticinella eubejaouaensis*[d] | tPe | 112.50 | 145.26 | 145.29 |
| F | FAD *Paraticinella eubejaouaensis*[d] | bTb | 114.30 | 148.28 | 149.87 |
| F | LAD *Globigerinelloides algerianus*[d] | tGa | 115.20 | 152.07 | 152.50 |

[a]Depth is reported in meters below seafloor (mbsf).
[b]Age estimate for FAD *Ticinella primula* from *Robaszynski and Caron* [1995] used as proxy for FAD *Ti. madecassiana* identified in Hole 1049A. See text for explanation of why the age for the FAD of *Ticinella primula* is used as a proxy for the FAD of *Ticinella madecassiana*.
[c]Depths for Hole 1049C from *Browning and Watkins* [2008]; age estimate from *Gradstein et al.* [2004].
[d]Depths for Hole 1049C from *Huber and Leckie* [2011a]; age estimates from *Gradstein et al.* [2004].

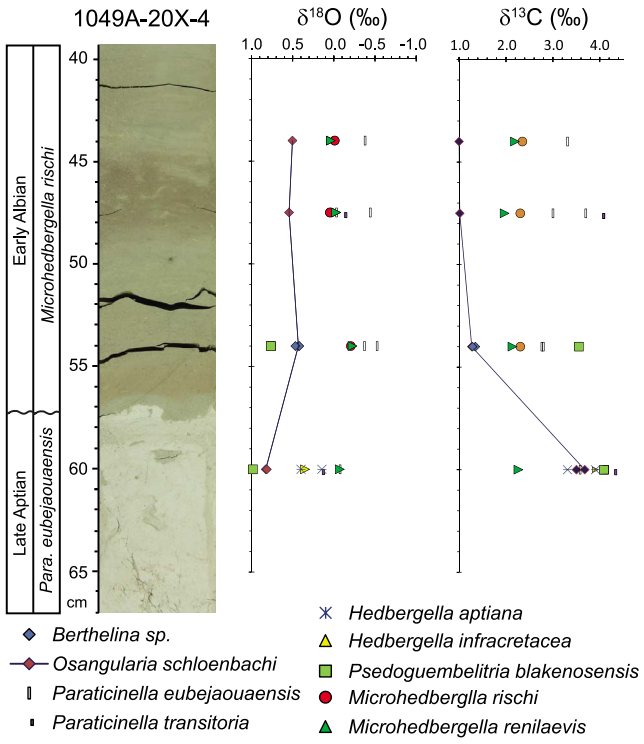


**Figure 6.** Oxygen and carbon isotope graphs across the Aptian/Albian boundary of core-section 1049A-20X-4, which is placed at the lithologic contact (57.5 cm). Note downward displacement of darker Albian sediment. Data presented in Table 4.

oceanographic mechanism. Rather, the abrupt geochemical shifts are best explained by the absence of a sediment record for the latest Aptian and/or earliest Albian as a result of erosion or non-deposition.

[23] One approach to estimating the duration of the unconformity is to construct an age model using the planktic foraminiferal and calcareous nannofossil biostratigraphic events listed in Table 6 and shown in Figure 8. Although ages for these events are cited from published sources, including the geomagnetic time scale of *Gradstein et al.* [2004], they are considered only as estimates, as none of the events have been directly calibrated using radiometric ages or geomagnetic tie points. Juxtaposition of the LAD of *Pa. eubejaouaensis* (112.5 Ma) and the FADs of *Hayesites albiensis* (111.69 Ma) and *Praediscosphaera columnata* (112.05 Ma) at the Aptian/Albian unconformity suggests that the duration of the unconformity is at least 0.84 m.y. (Figure 8 and Table 5). This interpretation is consistent with biostratigraphic evidence that the *Microhedbergella miniglobularis* Zone and the lowermost *Mi. rischi* Zone are missing from Site 1049 [*Huber and Leckie*, 2011a]. Using best fit lines of correlation through planktic foraminifer and calcareous nannofossil datums, sedimentation rates calculated from the Site 1049 age model are 2.98 m/m.y. for the lower Albian and 2.61 m/m.y. for the upper Aptian (Figure 8).

[24] An alternative way to estimate the extent of the unconformity is by correlating the Hole 1049C $\delta^{13}C$ record with the bulk carbonate $\delta^{13}C$ curve across the Aptian/Albian boundary at Pré-Guittard, Vocontian Basin using data generated by *Herrle et al.* [2004]. The latter section was judged to be stratigraphically continuous by *Kennedy et al.* [2000] and has been proposed as a candidate Global Boundary Stratotype Section (GSS) for the base of the Albian Stage. An interval yielding the highest late Aptian $\delta^{13}C$ values at Vocontian Basin, which occurs in the uppermost *Pa. eubejaouaensis* Zone (=*Ticinella bejaouaensis* Zone in previous works), was assigned to C-isotope Stage Ap-15 by *Herrle et al.* [2004] and is here correlated with an interval of high $\delta^{13}C$ values in the upper *Pa. eubejaouaensis* Zone of Hole 1049C (Figure 9). The break point where $\delta^{13}C$ values begin to decrease, at 223 m in the composite Vocontian Basin section, was identified by these authors as the C-isotope Ab-1/Ap-15 stage boundary and was proposed as a criterion for global correlation of the Aptian/Albian boundary, whereas we use the slightly higher extinction of *Pa. eubejaouaensis* to define the boundary [*Huber and Leckie*, 2011a].

[25] There are two intervals within early Albian C-isotope Stage Al-1 at the Vocontian Basin yielding quite low $\delta^{13}C$ values that could be correlated with the 2.5‰ negative excursion at Hole 1049C. One is the Niveau Kilian (~241 m in the composite section), which is a 1 m thick black shale that yields a 1.8‰ negative $\delta^{13}C$ excursion in bulk rock 11 m above the LO of *Pa. eubejaouaensis* [*Herrle et al.*, 2004]. The Kilian level also marks the horizon where large Aptian planktic foraminifer species become extinct (Caron, in work by *Kennedy et al.* [2000]; M. R. Petrizzo et al., Abrupt planktic foraminiferal turnover across the Niveau Kilian at Col de Pré-Guittard (Vocontian Basin, southeast France): New criteria for defining the Aptian/Albian boundary,

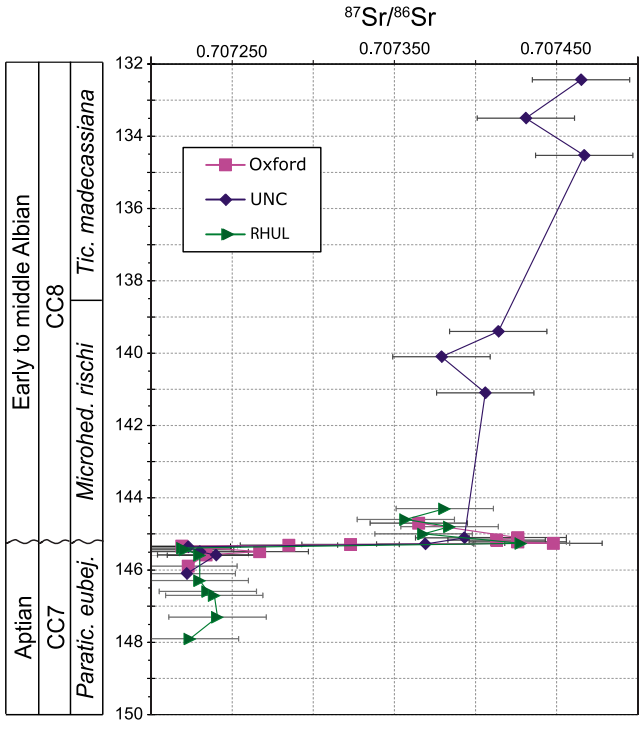


**Figure 7.** Sr isotope ratios from ODP Hole 1049C plotted relative to sample depth at Hole 1049C. Different symbols represent data generated from the Oxford, University of North Carolina (UNC) and Royal Holloway University (RHUL) geochemical laboratories.

**Table 6.** Strontium Isotope Ratio Data Obtained for Foraminifera From ODP Hole 1049C[a]

| Hole 1049C Sample | Depth[b] (mbsf) | Age[c] | $^{87}Sr/^{86}Sr$ UNC[d] | $^{87}Sr/^{86}Sr$ Oxford[e] | $^{87}Sr/^{86}Sr$ RHUL[f] | error | $^{87}Sr/^{86}Sr$ RHUL | error | $^{87}Sr/^{86}Sr$ RHUL | error |
|---|---|---|---|---|---|---|---|---|---|---|
| 11X-2, 124–126 | 132.44 | 107.42 | 0.707465 | | | | | | | |
| 11X-3, 80–82 | 133.50 | 107.77 | 0.707431 | | | | | | | |
| 11X-CC | 134.53 | 108.12 | 0.707467 | | | | | | | |
| 12X-1, 10–11 | 139.40 | 109.76 | 0.707414 | | | | | | | |
| 12X-1, 80–81 | 140.10 | 109.99 | 0.707379 | | | | | | | |
| 12X-2, 30–31 | 141.10 | 110.33 | 0.707406 | | | | | | | |
| 12X-4, 50–51 | 144.30 | 111.40 | | | 0.707381 | 9.00E-06 | | | | |
| 12X-4, 80–81 | 144.60 | 111.50 | | | 0.707357 | 1.00E-05 | | | | |
| 12X-4, 90–91 | 144.70 | 111.53 | | −0.000030 | | 1.10E-05 | | | | |
| 12X-4, 110–111 | 144.80 | 111.57 | | | 0.707384 | 1.40E-05 | | | | |
| 12X-4, 120–121 | 145.00 | 111.64 | | | 0.707368 | 1.00E-05 | | | | |
| 12X-4, 130–131 | 145.10 | 111.67 | | −0.000030 | | 1.70E-05 | | | | |
| 12X-4, 131–132 | 145.11 | 111.67 | 0.707393 | | | | | | | |
| 12X-4, 137–138 | 145.17 | 111.69 | | −0.000030 | | 1.20E-05 | | | | |
| 12X-4, 142–143 | 145.22 | 111.71 | | −0.000030 | | 1.40E-05 | | | | |
| 12X-4, 146–147 | 145.26 | 111.72 | | −0.000030 | 0.707428 | 7.67E-06 | 0.707452 | 1.10E-05 | 0.707404 | 1.20E-05 |
| 12X-4, 148–149 | 145.28 | 111.73 | 0.707369 | | | | | | | |
| 12X-4, 149–150 | 145.29 | 112.57 | | −0.000030 | | 1.40E-05 | | | | |
| 12X-5, 0–1 | 145.31 | 112.57 | | −0.000030 | | 1.10E-05 | | | | |
| 12X-5, 3–4 | 145.34 | 112.59 | | −0.000030 | | 1.30E-05 | | | | |
| 12X-5, 6–7 | 145.36 | 112.59 | 0.707223 | | | | | | | |
| 12X-5, 9–10 | 145.39 | 112.61 | | | 0.707220 | 1.05E-05 | 0.707240 | 1.00E-05 | 0.707199 | 1.10E-05 |
| 12X-5, 14–15 | 145.44 | 112.62 | | | 0.707221 | 9.00E-06 | | | | |
| 12X-5, 19–20 | 145.49 | 112.64 | 0.707230 | −0.000030 | | 9.00E-06 | | | | |
| 12X-5, 28–29 | 145.58 | 112.68 | | −0.000030 | | 6.40E-06 | | | | |
| 12X-5, 29–30 | 145.59 | 112.68 | 0.707240 | | 0.707230 | 9.00E-06 | | | | |
| 12X-5, 59–60 | 145.89 | 112.80 | | −0.000030 | | 1.00E-05 | | | | |
| 12X-5, 80–81 | 146.10 | 112.88 | 0.707222 | | | | | | | |
| 12X-5, 99–110 | 146.29 | 112.95 | | | 0.707230 | 1.00E-05 | | | | |
| 12X-5, 139–140 | 146.59 | 113.07 | | | 0.707235 | 1.15E-05 | 0.707230 | 1.20E-05 | 0.707240 | 1.10E-05 |
| 12X-6, 0–1 | 146.70 | 113.11 | | | 0.707239 | 1.40E-05 | | | | |
| 12X-6, 60–61 | 147.30 | 113.34 | | | 0.707241 | 1.10E-05 | | | | |
| 12X-6, 120–121 | 147.90 | 113.57 | | | 0.707224 | 1.20E-05 | | | | |

[a]Isotopic results are normalized to a value of 0.710 250 for NBS-987. Error for each analysis is 2SE. Note values for samples run at Oxford were consistently higher than corresponding analyses from the other labs, and this offset was corrected for in plotting Figure 10 (see text).
[b]Depth is reported in meters below seafloor (mbsf).
[c]Ages estimated using age model presented in Table 5 and Figure 9.
[d]University of North Carolina Chapel Hill; subtracted 0.000012 from raw values.
[e]Oxford University; added 0.000003 on raw values.
[f]Royal Holloway University in London; added 0.000002 on raw values.

submitted to *Newsletters on Stratigraphy*, 2011). The other level is a negative $\delta^{13}C$ shift about 30 m above the Kilian level (~271 m in the Vocontian Basin composite section and ~19 m below the Niveau Paquier).

[26] We propose that the $\delta^{13}C$ minimum immediately above the Aptian/Albian boundary at Site 1049 corresponds with the upper $\delta^{13}C$ minimum at 271 m within the C-isotope Stage Al-1 at the Vocontian Basin because of the absence at Site 1049 of the gradually decreasing $\delta^{13}C$ values that immediately follow the Kilian $\delta^{13}C$ excursion. If this correlation is correct, the age equivalent for the 41 m section spanning from uppermost C-isotope Stage Ap-15 (uppermost *Pa. eubejaouaensis* Zone) to the $\delta^{13}C$ minimum in upper C-isotope Stage Al-1 (middle *Mi. rischi* Zone = *Hd. planispira* Zone) at Vocontian Basin is missing at Site 1049. Using the mean sedimentation rate of 3 cm/ky estimated by *Herrle et al.* [2004] for the Vocontian Basin, the time missing is calculated as 1.37 m.y.

[27] A third approach to estimating the length of the hiatus is to use $^{87}Sr/^{86}Sr$ ratios relative to expected seawater values. Seawater $^{87}Sr/^{86}Sr$ ratios generally change slowly, but if the time is long or sampling density is high, this system can provide an independent check on the fidelity of the stratigraphic record [*MacLeod et al.*, 2001, 2003]. Applying this approach to the Sr data from Site 1049 suggests a hiatus that spans more than 4 million years (Figure 10), a conclusion at odds with both foraminiferal and nannofossil biostratigraphy and impossible to reconcile with the carbon isotope record. The Albian specimens are better preserved than Aptian specimens (whose values match those expected given their biostratigraphic age) arguing against a diagenetic explanation for the elevated early Albian ratios. A similar range of values have been reported for the early Albian in DSDP Site 511 [*Bralower et al.*, 1997] and were used in constraining the seawater curve for the Aptian/Albian boundary interval. Recent reinterpretation of the biostratigraphy at Site 511 [*Huber and Leckie*, 2011a] would shorten the interval of time over which the $^{87}Sr/^{86}Sr$ ratios increased at Site 511 and thus shorten the Sr-based estimate of the duration of the hiatus at 1049. If the seawater curve [*McArthur and Howarth*, 2004] is accurate and precise for the early Albian interval, a second alternative would be to suggest that the early Albian ocean was not well mixed with respect to strontium isotopes. Regardless, at present $^{87}Sr/^{86}Sr$ values do not help constrain the length of the hiatus in the study section.

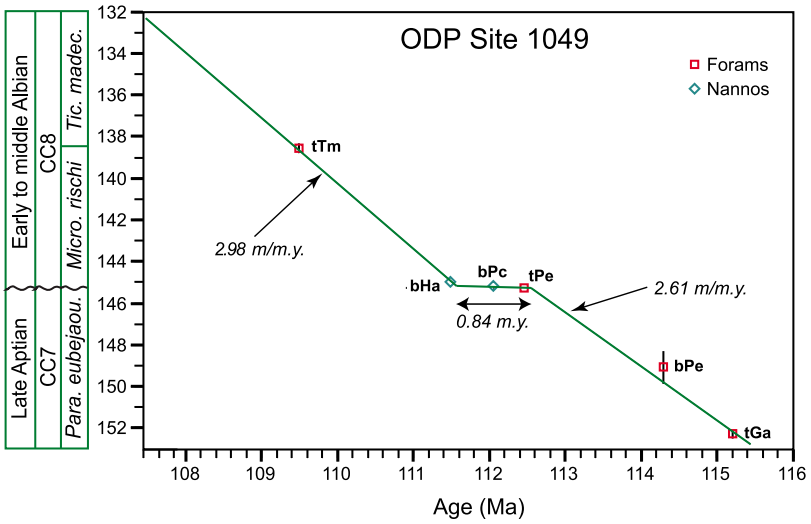


**Figure 8.** Age-depth model for the late Aptian–early Albian in ODP Site 1049. Vertical axis shows geologic age, calcareous nannofossil and planktic foraminiferal biozones, and meters below seafloor depth. Calculated sedimentation rates and duration of unconformity shown in italics. Stratigraphic uncertainty plotted as vertical bar for each datum with thickness between samples containing datum marker and next sample below or above where datum marker is absent. Full spelling and explanation of species data are presented in Table 5.

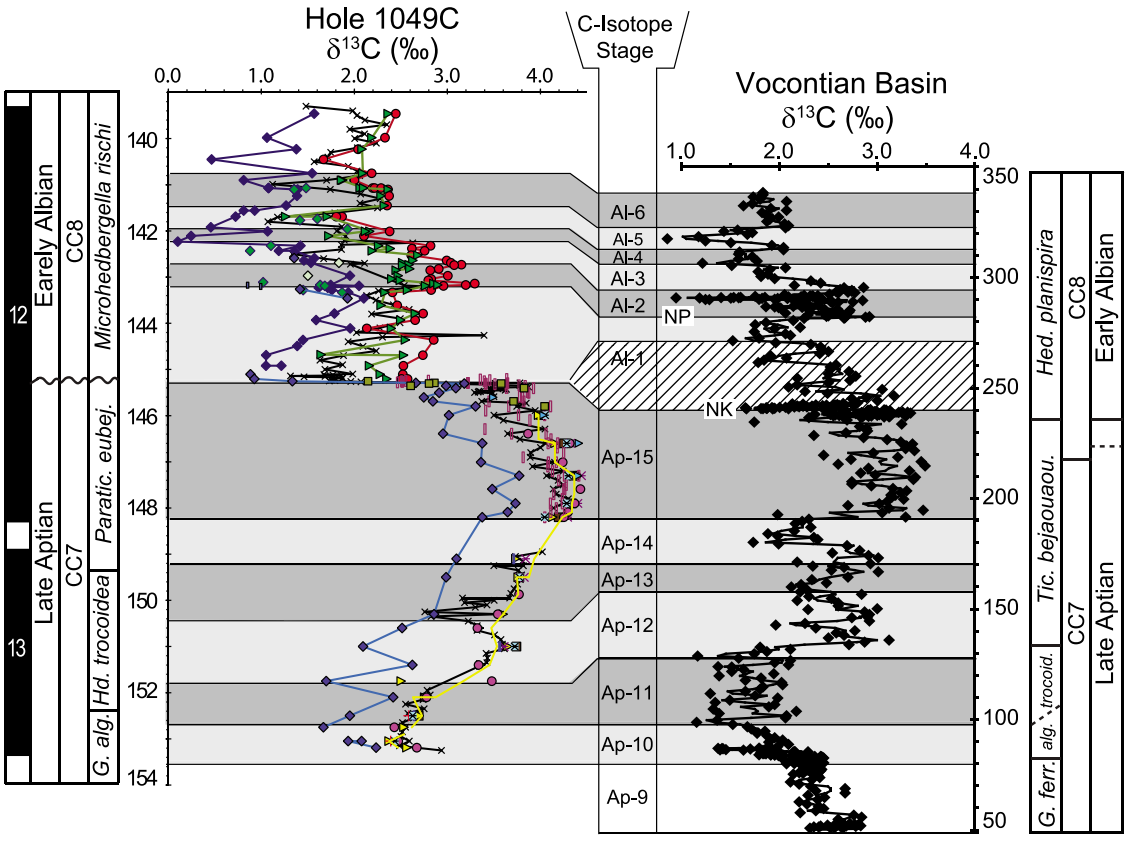


**Figure 9.** Correlation between the late Aptian–early Albian $\delta^{13}C$ record from Hole 1049C with the *Herrle et al.* [2004] bulk carbonate $\delta^{13}C$ data and isotope stages from the Vocontian Basin, in France. The diagonal pattern represents the stratigraphic interval in the Vocontian Basin that is interpreted as missing from Hole 1049C because of an unconformity. Note that the Aptian/Albian boundary of *Herrle et al.* [2004] has been shifted upward to correlate with the extinction of *Paraticinella eubejouaensis* (=*Ticinella bejaouaensis* of previous studies). See Figure 4 caption for key to symbols.

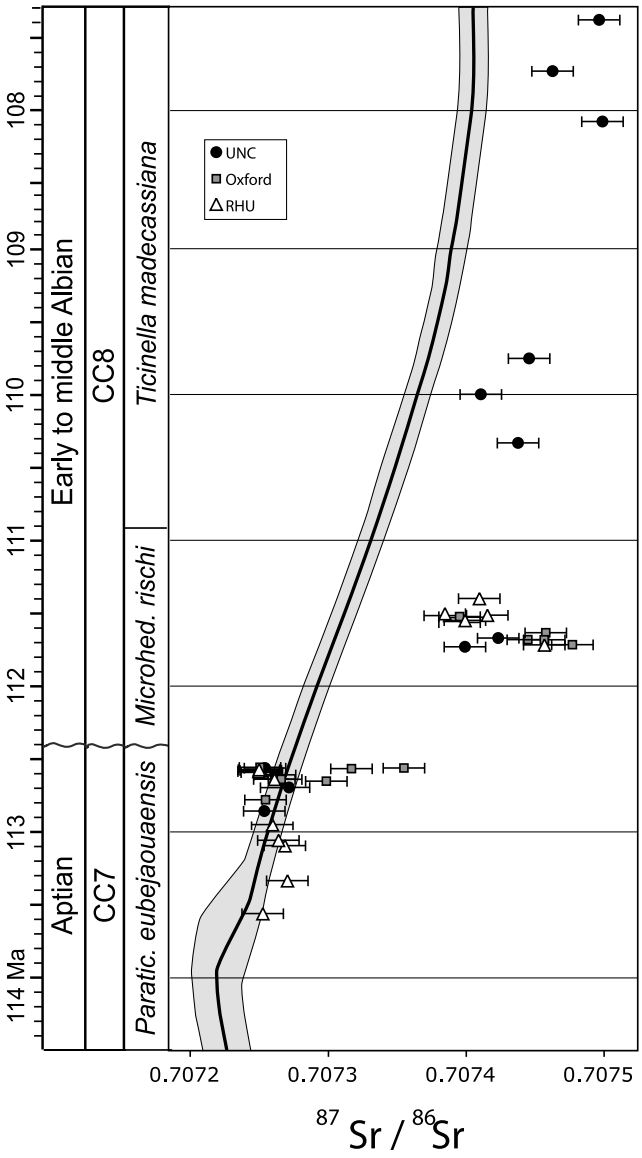


**Figure 10.** Sr isotope ratios from ODP Hole 1049C plotted relative to the global seawater curve of *McArthur and Howarth* [2004] using sample age estimates that are based on an age model constructed in Figure 8 and Table 5. See Figure 7 caption for explanation of abbreviations and Table 6 for data.

### 5.2. Evidence for Reworking and Bioturbation

[28] Faunal changes are dramatic across the boundary, but Aptian species are present in low numbers in the first 10 cm above the Aptian/Albian contact at Site 1049 and Albian taxa are present in low abundances in samples a few cm below the contact [*Huber and Leckie*, 2011a]. These anomalous occurrences are judged to be the result of reworking rather than species survivorship based on intra and interspecies comparisons of the carbon isotope signatures. In Hole 1049 C the Aptian planktic species *Pa. eubejaouaensis* shows essentially no difference in $\delta^{13}$C values across the boundary, with uppermost Aptian specimens averaging 3.6‰, and lowermost Albian specimens averaging 3.5‰ (Table 1 and Figure 5). Other Aptian planktic species (*Pa. transitoria* and *Pseudoguembelitria blakenosensis*) present in the basal Albian in Hole 1049A also show little change in their $\delta^{13}$C values across the boundary (Table 4 and Figure 6). Similarly, specimens of the Albian species *Mi. renilaevis* that occur below the boundary contact at Site 1049 have a $\delta^{13}$C value that is much lower than those seen in co-occurring Aptian planktic specimens but within 0.2‰ of the average value obtained from the lower Albian specimens (Table 4 and Figure 6). That is, suspect taxa show no change in $\delta^{13}$C across the boundary. In contrast, the benthic foraminifer *Osangularia schloenbachi*, which is common in the upper Aptian and lower Albian samples, shows a 2.5‰ negative shift across the interval. Bioturbation, including burrow fill below the boundary that appears similar to the chalk above the boundary, provides a mechanism to explain the apparent reworking whereas the change in the $\delta^{13}$C values of *Osangularia schloenbachi* and *Berthelina* spp. indicates the $\delta^{13}$C represents a shift in the isotopic composition of contemporaneous seawater. Oxygen isotopic ratios are consistent with this conclusion but provide little additional resolution due to the small changes in $\delta^{18}$O ratios across the interval, but the presence of specimens reworked both up and down across the boundary in the mixed assemblages analyzed would explain the smooth (albeit steep) increase in $^{87}$Sr/$^{86}$Sr across the boundary.

### 5.3. Paleotemperature and Paleosalinity Inferences

[29] As noted in the introduction, a major contribution of this study was an effort to provide paleotemperature estimates for the Aptian/Albian interval using $\delta^{18}$O measurements of well-preserved ('glassy' in the Albian and 'frosty' in the Aptian) specimens. At face value, though, our estimated temperatures are problematically cool. Calculated temperatures are 10–16°C cooler than modern temperatures in the same region whereas paleoclimatic proxy data and climate model predictions for the mid-Cretaceous indicate that subtropical sea surface temperatures should have been the same as or warmer than at present [*Frakes*, 1999; *Royer*, 2006]. This difference suggests a significant contribution from diagenetic overprints, high seawater $\delta^{18}$O values, overestimates in predicted mid-Cretaceous temperatures, and/or some combination of these.

[30] In the late Aptian interval, diagenesis almost certainly contributes to the positive $\delta^{18}$O values. The specimens are recrystallized (Figures 3c and 3d), both bulk carbonate (assumed to be composed dominantly of nannofossils) and the more delicate planktic foraminifera have values near or above benthic values in the same sample, and only the more robust planktic taxa have values consistently lower than benthic values (Figure 4). These observations can be explained by convergence of the $\delta^{18}$O values in all taxa moving toward a diagenetic, $\delta^{18}$O end-member with values slightly higher than that of the benthic foraminifera [*Pearson et al.*, 2001]. Bulk carbonate and the more delicate planktic foraminifera express this overprint more strongly than the more robust planktic taxa and the benthic taxa.

[31] A diagenetic explanation, however, is not tenable for the younger samples where preservation is excellent (Figures 3a and 3b) and the rank ordering of $\delta^{18}$O values among taxa is both intuitively correct and remarkably consistent (Figure 4). Outside of OAE1b, the lowest planktic values are consistently $\sim -1$‰ and benthic values are

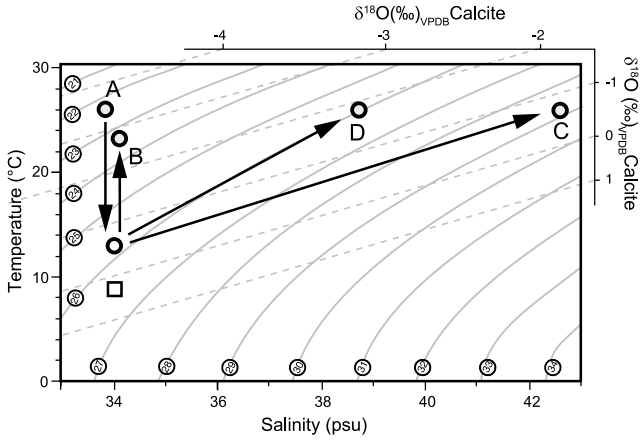


**Figure 11.** Temperature-salinity-density diagram with isopleths of calcite $\delta^{18}O$ (dashed lines) using a slope of 0.35‰/psu [*Railsback et al.*, 1989] and assuming an ice-free salinity S = 34 psu, an ice-free mean ocean water composition $\delta^{18}O_w = -1‰$. Numbers in circles label isopycnals and are expressed as $\sigma_t$ units. Early Albian glassy benthic (square) and planktic (circle) $\delta^{18}O$ values averaged from above and below the black shale interval are plotted. The mean planktic $\delta^{18}O$ requires vector A, 3.0‰ diagenetic overprint if 26°C is assumed for the mean annual sea surface temperature during the early Albian; vector B, a increase of >2‰ if glacial ice resulted in high $\delta^{18}O_w$ values and 23°C is assumed for the mean annual sea surface temperature during the early Albian; vector C, S = 42 psu using an evaporation gradient of $\delta^{18}O = -0.35‰$/psu (dashed lines) if 26°C is assumed for the mean annual sea surface temperature during the early Albian; or vector D, S = 38.8 psu using a −0.65‰/psu evaporation gradient (averaged North Atlantic tropical surface waters, isopleths not plotted but would largely parallel vector D). Only model D is considered a plausible explanation for Albian foraminiferal $\delta^{18}O$ values (see text).

between 0‰ and 0.5‰ (Figure 4) and we use these values to evaluate different oceanographic scenarios (Figure 11). The seasonal temperature variation in the upper 50 m at 25°N in the modern western North Atlantic is 24–28°C (National Oceanographic Data Center: http://iridl.ldeo.columbia.edu/descriptions/.nasa1234.html), whereas calculated temperatures for a planktic foraminifera of $-1‰_{PDB}$ and assuming an ice-free Cretaceous seawater $\delta^{18}O$ value of $-1‰_{SMOW}$ are ∼15°C [*Bemis et al.*, 1998]. Considering evidence for cool conditions at high latitudes during the Early Cretaceous [*Kemper*, 1987; *Frakes et al.*, 1992; *Pirrie et al.*, 1995, 2004; *Ferguson et al.*, 1999; *Price*, 1999] a comparison to the modern ocean seems a more conservative option than invoking greenhouse temperatures of the Late Cretaceous. If the high planktic values were attributed solely to alteration of calcite formed at 26°C in water with a $\delta^{18}O$ value of $-1‰_{SMOW}$, the diagenetic overprint would have shifted the initial value by ∼3‰ (vector A in Figure 11). A shift of this magnitude would require replacement of >75% of the original calcite with recrystallized calcite of the same isotopic composition as the co-occurring benthic foraminifera without any visual evidence of alteration (Figures 3a and 3b). In contrast, more modest diagenetic overprints correlate with readily apparent recrystallization in other deep-sea cores [*Pearson et al.*, 2001].

[32] A similar scaling argument can be used to dismiss explanations invoking glacial effects. Even allowing the maximum cooling of 3°C (that is, assuming a sea surface temperature of 23°C) estimated for this latitude during the last glacial maximum [*Waelbroeck et al.*, 2009], a glacial ice effect would have had to have resulted in a >2‰ increase in seawater $\delta^{18}O$ values (vector B in Figure 11). This increase, assuming no significant change in the mass or isotopic composition of the hydrosphere and an average $\delta^{18}O$ value of the hypothetical glacial ice of $-30‰_{SMOW}$, would correspond to an ice volume similar to that at the last glacial maximum during the early Albian, a time for which no clear glacial indicators have been reported.

[33] Regional explanations invoking the "salinity" effect also seem impossible when using standard assumptions. Because of the fractionation between water and water vapor, evaporation results in an increase of the $\delta^{18}O$ values of local seawater as well as an increase in salinity. To examine the role of this effect in explaining foraminifer $\delta^{18}O$ values for Cretaceous samples, researchers have generally followed *Railsback et al.* [1989] in using a slope of ∼0.35‰/psu during evaporative concentration of seawater [e.g., *Woo et al.*, 1992; *MacLeod and Huber*, 1996]. Applying this relationship to the data from Site 1049 would result in salinities in excess of 42 psu for surface water of 26°C in equilibrium with foraminiferal calcite of $-1‰_{PDB}$ (vector C in Figure 11). At 42 psu, this surface water would be considerably denser than the bottom waters inferred from a benthic $\delta^{18}O$ value of $0.2‰_{PDB}$ in the same temperature/salinity plot. Such water column structure with a reversed density pattern is physically impossible. However, we note that the slope of ∼0.35‰/psu generally used is based on the average observed slopes for Mediterranean and Red Sea surface waters whereas the compilation showed a range of slopes varying from 0.63‰/psu for North Atlantic Surface Water to 0.12‰/psu for Atlantic Equatorial Surface Water [*Railsback et al.*, 1989].

[34] Using the value of 0.63‰/psu results in salinities of ∼38.8 psu for surface water of 26°C in equilibrium with foraminiferal calcite of $-1‰_{PDB}$ (vector D in Figure 11). The density of this water would not be greater than that estimated from bottom water using the benthic $\delta^{18}O$ value. The slope of the seawater $\delta^{18}O$/salinity trend is not simple to interpret, but is expected to be high when kinetic fractionation plays a large role in the effective fractionation and the water vapor is efficiently transported away from the site of evaporation with minimal return precipitation. Given the estimated paleolatitude of ∼25°N for Site 1049 [*Ogg and Bardot*, 2001] on the western side of the North Atlantic, vapor exported from the North Atlantic basin would likely be transported with the trade winds into the Pacific, which could have been partly isolated from the proto-Atlantic, a situation reminiscent of the present-day moisture transport across Central America away from the Caribbean Sea [*Leduc et al.*, 2007] (Figure 12).

### 5.4. Basin Geography and Strontium Isotopes

[35] Considering both the anomalous Sr isotopic values and the oxygen isotope values requiring large changes in local seawater composition, we invoke paleogeography as a

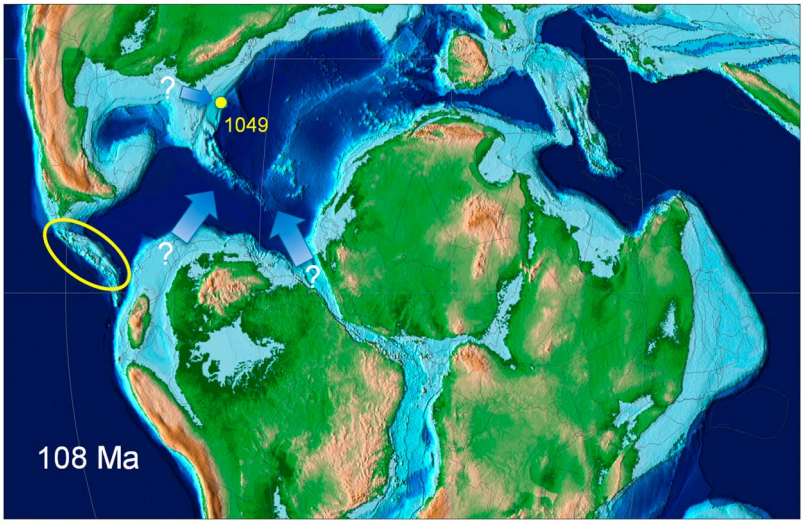


**Figure 12.** Paleogeographic reconstruction for 108 Ma showing the low to middle latitude region of the Western Hemisphere, the configuration of the North Atlantic basin, areas of the continents that were flooded by the ocean, and the location of ODP Site 1049. Possible sources for warm, saline deep-water masses are shown by arrows. Ventilation of the western North Atlantic into the Pacific Ocean was probably restricted by a shallow sill following the Central American island arc. Albian Paleogeographic map by C. R. Scotese, © 2011, PALEOMAP Project (C. R. Scotese, The PALEOMAP Project PaleoAtlas for ArcGIS, vol. 2, Cretaceous Paleogeographic and Plate Tectonic Reconstructions, version 9.2r, PALEOMAP Project, Arlington, Texas, 2011).

major controlling variable in the paleoceanographic evolution of the North Atlantic basin during the Aptian/Albian. The North Atlantic was a substantial basin at that time, but may have had limited connections to adjacent ocean basins (Figure 12). Rifting between South America and Africa during the Early Cretaceous created initially discontinuous marine basins with thick accumulations of siliciclastic sediments and evaporites [*Natland*, 1978; *Rabinowitz and LaBrecque*, 1979; *Tucholke and Vogt*, 1979; *Jones et al.*, 1995]. As rifting continued the basins widened, deepened and became permanently interconnected with the North Atlantic between the late Aptian and early Albian [*Moullade et al.*, 1998; *Pletsch et al.*, 2001; *Moulin et al.*, 2010]. Regional hiatuses in the Albian of the North Atlantic [*Pletsch et al.*, 2001], including the Aptian/Albian boundary unconformity at Blake Nose, may provide evidence of episodic outflow from this incipient ocean basin.

[36] If efficient vapor transport from the North Atlantic inferred from the stable isotopic composition of planktic foraminifera (Figure 11) indicates the early Albian hydrological cycle was enhanced (similar to suggested Late Cretaceous conditions [*Erbacher et al.*, 2001; *White et al.*, 2001; *Ufnar et al.*, 2004]), high rates of precipitation coupled with high temperatures would have caused high rates of chemical weathering in tropical South America and Africa. Runoff carrying the products of this weathering, including a continental $^{87}Sr/^{86}Sr$ signature, may initially have been largely trapped in the discontinuous central Atlantic rift basins. The continental Sr would have increasingly reached the North Atlantic as central Atlantic connectivity improved, and the effect on the North Atlantic Sr budget would have been greatest if connections to other basins were quite restricted (Figure 12).

[37] The degree of restriction needed, though, is formidable. The increase in $^{87}Sr/^{86}Sr$ of ~0.000 200 across Aptian/Albian boundary hiatus and the ~0.000 100 difference between the early Albian values at Hole 1049 and the seawater curve (Figure 10) are large. Despite limited connections with the Red Sea and North Atlantic, the Mediterranean has an $^{87}Sr/^{86}Sr$ composition the same as the global ocean, and modeling results suggest that a tripling of the river influx and severe basin isolation are required to explain the 0.001 000 to 0.004 000 difference between Mediterranean $^{87}Sr/^{86}Sr$ values and contemporaneous global seawater values during the Messinian Salinity Crisis [*Topper et al.*, 2011]. While the North Atlantic Albian offsets are an order of magnitude smaller than Messinian offsets, simple calculations of the Sr budget still imply significant restriction. Assuming the measured North Atlantic $^{87}Sr/^{86}Sr$ value of ~0.7074 at ~112 Ma is a mixture of global seawater with a ratio of ~0.7073 (Figure 10) and riverine input at 0.7119 [*Palmer and Edmond*, 1989], 2.2% of the Sr in the basin would need to come from runoff. Using a basin volume between 6.3 and $9.9 \times 10^7$ km$^3$ and riverine input between 4300 and 6500 km$^3$/yr [*Zhou et al.*, 2008; J. Zhou and C. J. Poulsen, personal communication, 2011], and Sr concentrations of seawater and riverine input at 7.9 mg/l and 0.078 mg/l, respectively [*Palmer and Edmund*, 1989], the Sr inventory of the North Atlantic would have been between 5.0 and $7.8 \times 10^{20}$ mg and the riverine flux would have been between 3.4 and $5.0 \times 10^{14}$ mg/yr. Dividing the inventory by the total Sr flux in (of which riverine input is estimated at 2.2%), gives an estimated residence time of Sr in the basin of 20,000 to 50,000 years. Calculated residence times vary linearly with the input parameters, so meaningfully reducing the calculated residence time requires large departures from the values used

in our calculations. Once Sr fluxes are estimated, it is also possible to estimate the water balance in the basin. Because Sr would leave with outflow but not with evaporation and assuming no internal Sr sinks, the volume of seawater flowing out of the basin would equal the total Sr flux in divided by seawater Sr concentration. The result of this calculation is an outflow between 2000 and 3000 $km^3$/yr or about half the flow of the Amazon. Taking the difference between this outflow estimate and the sum of riverine and marine flow into the basin suggests ~70% of the water leaving the North Atlantic basin would needed to have done so through evaporation.

[38] In short, this analysis suggests if restriction alone explains the observed $^{87}Sr/^{86}Sr$ offset between the North Atlantic samples and the seawater curve, the North Atlantic would have been connected to the world's oceans by annual flow rates less than that of the modern Amazon River. Evaporation would have needed to closely balance runoff into the basin with salinity not exceeding the 42 to 49 psu tolerance limits of modern planktic foraminifera [*Bijma et al.*, 1990]. Deep circulation would have needed to be effectively disconnected from the global ocean but have been vigorous enough to ventilate the deep basin for most of the Albian (given the dominance of bioturbation in North Atlantic bathyal sediments). Finally, surface connections must have been sufficient to allow free exchange among Albian planktic foraminiferal assemblages [e.g., *Huber and Leckie*, 2011a].

[39] Such a scenario is consistent with patterns in Albian modeling results [*Poulsen et al.*, 2001] and decoupling of Sr isotopic and salinity trends in the Neogene Mediterranean record [*Flecker et al.*, 2002], but it also seems quite severe. If errors in the values used to estimate the Sr and water budget ($^{87}Sr/^{86}Sr$ ratio of riverine input, riverine Sr concentration, riverine flow, basin volume) consistently bias the calculation against resolving continental contributions, the degree of isolation and the estimated importance of evaporation would be reduced. Alternatively, inaccuracy in details of the age models and/or Sr data used to generate the Albian portion of the Sr-isotope global seawater curve might increase the apparent offset of North Atlantic values. These two possibilities are not mutually exclusive. The question could be resolved by restudying the material used to generate the Sr curve or more detailed modeling of the North Atlantic basin. More interesting to a general understanding of the evolution of Aptian/Albian earth systems, though, is how change in evaporation, runoff, and the degree of North Atlantic restriction might have contributed to the carbon isotopic decrease, apparent temperature increase, and global foraminiferal extinctions across the Aptian/Albian boundary interval. Unfortunately, the hiatus at Site 1049 and absence of a more complete Aptian/Albian boundary record in the North Atlantic compromise efforts to address this question further.

## 6. Summary and Conclusions

[40] Biostratigraphic and chemostratigraphic correlation of the Aptian–Albian boundary interval at ODP Site 1049 suggest that this sequence spans from 115 to 108 Ma with a hiatus ranging from 0.8 to 1.4 m.y in duration across the boundary itself. Abrupt shifts in lithology, faunal assemblages, and geochemistry across the boundary level confirm the presence of this hiatus. Despite these sedimentological complications, strontium isotopic results suggest the existing sea level curve has values that are too low through the Albian Stage.

[41] The glassy shell preservation of early Albian foraminifera and the unusually good preservation of the late Aptian foraminifera enable construction of a framework for interpreting North Atlantic paleoceanography before and after the terminal Aptian foraminiferal extinction event and across the Oceanic Anoxic Event (OAE) 1b. Using standard assumptions for Cretaceous isotopic paleotemperature calculations, mid-bathyal benthic foraminifer $\delta^{18}O$ values indicate that late Aptian-middle Albian bottom waters were mostly 8–10°C, a range that is similar to bottom temperatures calculated for the late Campanian–middle Maastrichtian at Blake Nose [*MacLeod and Huber*, 2001]. Similar calculations for planktic taxa yield anomalously cool temperatures that cannot be explained by diagenesis, growth of a polar ice cap, or standard calculations for the isotopic consequences of excess evaporation. However, the values are compatible with reasonable temperatures (~26°C) if vapor export during evaporation was efficient. This climatic regime in combination with evolving Atlantic paleogeography could explain the carbon, oxygen shifts and the planktic foraminifer extinction event associated with the transition from the Aptian to the Albian. Specifically, our results imply that attempts to interpret proxy signals from the proto North Atlantic need to consider a much greater degree of isolation of the basin than previously suggested, but resolving cause and effect relationships will require study of sections that are both complete and contain excellent preservation.

[42] **Acknowledgments.** This research used samples and data provided by the Integrated Ocean Drilling Program (IODP). IODP is sponsored by the U.S. National Science Foundation (NSF) and participating countries under the management of IODP Management International. We thank N. Price for assistance with picking of some stable isotope samples, C. Scotese for the use of the map in Figure 12, and C. Kelley, E. Martin, C. Poulsen, and J. Zhou for useful discussions and reviews. The manuscript benefited significantly from critical reviews by R. Norris and an anonymous reviewer and editorial suggestions from C. Charles. This study was supported by the Smithsonian Institution Walcott Fund to BTH and NSF EAR 640171 to BTH and NSF OCE 022071 to KMG. This research was also made possible by an NSERC (288321) and NERC (NE/H021868/1) grant to DRG.

## References

Barker, C. E., M. Pawlewicz, and E. A. Cobabe (2001), Deposition of sedimentary organic matter in black shale facies indicated by the geochemistry and petrography of high-resolution samples, Blake Nose, western North Atlantic, *Geol. Soc. Spec. Publ.*, *183*, 49–72.

Bemis, B. E., H. J. Spero, J. Bijma, and D. W. Lea (1998), Reevaluation of the oxygen isotopic composition of planktonic foraminifera: Experimental results and revised paleotemperature equations, *Paleoceanography*, *13*, 150–160, doi:10.1029/98PA00070.

Benson, W. E., et al. (1978), *Initial Reports of the Deep Sea Drilling Project*, vol. 44, U.S. Gov. Print. Off., Washington, D. C., doi:10.2973/dsdp.proc.44.1978.

Bijma, J., W. W. Faber Jr., and C. Hemleben (1990), Temperature and salinity limits for growth and survival of some planktonic foraminifers in laboratory cultures, *J. Foraminiferal Res.*, *20*, 95–116, doi:10.2113/gsjfr.20.2.95.

Bralower, T. J., P. D. Fullagar, C. K. Paull, G. S. Dwyer, and R. M. Leckie (1997), Mid-Cretaceous strontium-isotope stratigraphy of deep-sea sections, *Geol. Soc. Am. Bull.*, *109*, 1421–1442, doi:10.1130/0016-7606(1997)109<1421:MCSISO>2.3.CO;2.

Browning, E. L., and D. K. Watkins (2008), Elevated primary productivity of calcareous nannoplankton associated with ocean anoxic event 1b during the Aptian/Albian transition (Early Cretaceous), *Paleoceanography*, *23*, PA2213, doi:10.1029/2007PA001413.

Clarke, L. J., and H. C. Jenkyns (1999), New oxygen isotope evidence for long-term Cretaceous climatic change in the Southern Hemisphere, *Geology*, *27*, 699–702, doi:10.1130/0091-7613(1999)027<0699:NOIEFL>2.3.CO;2.

Dutton, A. L., B. T. Huber, K. C. Lohmann, and W. J. Zinsmeister (2007), High-resolution stable isotope profiles of a dimitobellid belemnite: Implications for paleodepth habitat and late Maastrichtian climate seasonality, *Palaios*, *22*, 642–650.

Erbacher, J., B. T. Huber, R. D. Norris, and M. Markey (2001), Increased thermohaline stratification as a possible cause for an oceanic anoxic event in the Cretaceous Period, *Nature*, *409*, 325–327, doi:10.1038/35053041.

Ferguson, K. M., R. T. Gregory, and A. Constantine (1999), Lower Cretaceous (Aptian–Albian) secular changes in the oxygen and carbon isotope record from high paleolatitude, fluvial sediments, southeast Australia: Comparisons to the marine record, in *Evolution of the Cretaceous Ocean-Climate System*, *Spec. Pap.*, vol. 332, edited by E. Barrera and C. C. Johnson, pp. 59–72, Geol. Soc. of Am., Boulder, Colo.

Flecker, R., S. de Villiers, and R. Ellam (2002), Modelling the effect of evaporation on the salinity-$^{87}Sr/^{86}Sr$ relationship in modern and ancient marginal-marine systems, *Earth Planet. Sci. Lett.*, *203*, 221–233, doi:10.1016/S0012-821X(02)00848-8.

Frakes, L. A. (1999), Estimating the global thermal state from Cretaceous sea surface and continental temperature data, in *Evolution of the Cretaceous Ocean-Climate System*, *Spec. Pap.*, vol. 332, edited by E. Barrera and C. C. Johnson, pp. 49–57, Geol. Soc. of Am., Boulder, Colo.

Frakes, L. A., J. E. Francis, and J. I. Syktus Climate (1992), *Climate Modes of the Phanerozoic*, 274 pp., Cambridge Univ. Press, Cambridge, U. K., doi:10.1017/CBO9780511628948.

Gradstein, F. M., J. G. Ogg, and A. G. Smith (2004), *A Geologic Time Scale 2004*, 589 pp., Cambridge Univ. Press, Cambridge, U. K.

Hay, W. W., et al. (1999), Alternative global Cretaceous paleogeography, in *Evolution of the Cretaceous Ocean-Climate System*, *Spec. Pap.*, vol. 332, edited by E. Barrera and C. Johnson, pp. 1–47, Geol. Soc. of Am., Boulder, Colo.

Herrle, J. O., P. Kößler, O. Friedrich, H. Erlenkeuser, and C. Hemleben (2004), High-resolution carbon isotope records of the Aptian to Lower Albian from SE France and the Mazagan Plateau (DSDP Site 545), A stratigraphic tool for paleoceanographic and paleobiologic reconstruction, *Earth Planet. Sci. Lett.*, *218*, 149–161, doi:10.1016/S0012-821X(03)00646-0.

Holbourn, A., and W. Kuhnt (2001), No extinctions during oceanic anoxic event 1b: The Aptian–Albian benthic foraminiferal record of ODP Leg 171, *Geol. Soc. Spec. Publ.*, *183*, 73–92.

Huber, B. T., and R. M. Leckie (2011a), Planktic foraminiferal species turnover across deep-sea Aptian/Albian boundary sections, *J. Foraminiferal Res.*, *41*, 53–95, doi:10.2113/gsjfr.41.1.53.

Huber, B. T., and R. M. Leckie (2011b), Errata: Planktic foraminiferal species turnover across deep-sea Aptian/Albian boundary sections, *J. Foraminiferal Res.*, *41*, 196.

Jones, E. J. W., S. C. Cande, and F. Spathopoulos (1995), Evolution of a major oceanographic pathway: The equatorial Atlantic, *Geol. Soc. Spec. Publ.*, *90*, 199–213.

Kemper, E. (1987), Das Klima der Kreide-Zeit, *Geol. Jahrb. Reihe A*, *96*, 5–185.

Kennedy, W. J., A. S. Gale, P. R. Bown, M. Caron, R. J. Davey, D. Gröcke, and D. S. Wray (2000), Integrated stratigraphy across the Aptian–Albian boundary in the Marnes Bleues, at the Col de Pré-Guittard, Arnayon (Drôme), and at Tartonne (Alpes-de-Haute-Provence), France: A candidate Global Boundary Stratotype Section and Boundary Point for the base of the Albian Stage, *Cretaceous Res.*, *21*, 591–720, doi:10.1006/cres.2000.0223.

Kuypers, M. M. M., P. Blokker, J. Erbacher, H. Kinkel, R. D. Pancost, S. Stefan Schouten, and J. S. Sinninghe Damsté (2001), Massive expansion of marine archaea during a mid-Cretaceous Oceanic Anoxic Event, *Science*, *293*, 92–95, doi:10.1126/science.1058424.

Leckie, R. M., T. J. Bralower, and R. Cashman (2002), Oceanic anoxic events and plankton evolution: Biotic response to tectonic forcing during the mid-Cretaceous, *Paleoceanography*, *17*(3), 1041, doi:10.1029/2001PA000623.

Leduc, G., L. Vidal, K. Tachikawa, F. Rostek, C. Sonzogni, L. Beaufort, and E. Bard (2007), Moisture transport across Central America as a positive feedback on abrupt climatic changes, *Nature*, *445*, 908–911, doi:10.1038/nature05578.

MacLeod, K. G., and B. T. Huber (1996), Reorganization of deep ocean circulation accompanying a Late Cretaceous extinction event, *Nature*, *380*, 422–425, doi:10.1038/380422a0.

MacLeod, K. G., and B. T. Huber (2001), The Maastrichtian record at Blake Nose (western Atlantic) and implications for global paleoceanographic and biotic changes, *Geol. Soc. Spec. Publ.*, *183*, 111–130.

MacLeod, K. G., B. T. Huber, and P. D. Fullagar (2001), Evidence for a small (~0.000030) but resolvable increase in seawater $^{87}Sr/^{86}Sr$ ratios across the Cretaceous-Tertiary boundary, *Geology*, *29*, 303–306, doi:10.1130/0091-7613(2001)029<0303:EFASBR>2.0.CO;2.

MacLeod, K. G., P. Fullagar, and B. T. Huber (2003), $^{87}Sr/^{86}Sr$ test of the degree of impact-induced slope failure in the Maastrichtian of the western North Atlantic, *Geology*, *31*, 311–314, doi:10.1130/0091-7613(2003)031<0311:SSTOTD>2.0.CO;2.

McArthur, J. M., and R. J. Howarth (2004), Strontium isotope stratigraphy, in *Geological Timescale 2004*, edited by J. G. Ogg, F. M. Gradstein, and A. G. Smith, pp. 1–589, Cambridge Univ. Press, Cambridge.

Moulin, M., D. Aslanian, and P. Unternehr (2010), A new starting point for the South and equatorial Atlantic Ocean, *Earth Sci. Rev.*, *98*, 1–37, doi:10.1016/j.earscirev.2009.08.001.

Moullade, M., et al. (1998), Mesozoic biostratigraphic, paleoenvironmental and paleobiogeographic synthesis, equatorial Atlantic, *Proc. Ocean Drill. Program Sci. Results*, *159*, 481–490.

Natland, J. H. (1978), Composition, provenance, and diagenesis of Cretaceous clastic sediments drilled on the Atlantic continental margin off southern Africa, DSDP 361–implications for the early circulation of the South Atlantic, *Initial Rep. Deep Sea Drill. Proj.*, *40*, 1025–1061.

Norris, R. D., D. Kroon, and A. Klaus (1998), *Proceedings of the Ocean Drilling Program, Initial Reports*, vol. 171B, 749 pp., Ocean Drill. Program, College Station, Tex.

Ogg, J. G., and L. Bardot (2001), Aptian through Eocene magnetostratigraphic correlation of the Blake Nose transect (Leg 171B), Florida continental margin [online], *Proc. Ocean Drill. Program Sci. Results*, *171B*, 58 pp., doi:10.2973/odp.proc.sr.171b.104.2001. [Available at http://www-odp.tamu.edu/publications/171B_SR/chap_09/chap_09.htm.]

Palmer, M. R., and J. M. Edmond (1989), The strontium isotope budget of the modern ocean *Earth Planet. Sci. Lett.*, *92*, 11–26, doi:10.1016/0012-821X(89)90017-4.

Pearson, P. N., P. W. Ditchfield, J. Singano, K. G. Harcourt-Brown, C. J. Nicholas, R. K. Olsson, N. J. Shackleton, and M. A. Hall (2001), Warm tropical sea surface temperatures in the Late Cretaceous and Eocene epochs, *Nature*, *413*, 481–487, doi:10.1038/35097000.

Pirrie, D., P. Doyle, J. D. Marshall, and G. Ellis (1995), Cool Cretaceous climates: New data from the Albian of Western Australia, *J. Geol. Soc.*, *152*, 739–742, doi:10.1144/gsjgs.152.5.0739.

Pirrie, D., J. D. Marshall, P. Doyle, and A. C. Riccardi (2004), Cool early Albian climates: New data from Argentina, *Cretaceous Res.*, *25*, 27–33, doi:10.1016/j.cretres.2003.10.002.

Pletsch, T., J. Erbacher, A. E. L. Holbourn, W. Kuhnt, M. Moullade, F. E. Oboh-Ikuenobede, E. Söding, and T. Wagner (2001), Cretaceous separation of Africa and South America: The view from the West African margin (ODP Leg 159), *J. South Am. Earth Sci.*, *14*, 147–174, doi:10.1016/S0895-9811(01)00020-7.

Poulsen, C. J., E. J. Barron, M. A. Arthur, and W. H. Peterson (2001), Response of the mid-Cretaceous global oceanic circulation to tectonic and $CO_2$ forcings, *Paleoceanography*, *16*(6), 576–592, doi:10.1029/2000PA000579.

Premoli Silva, I., and W. V. Sliter (1999), Cretaceous paleoceanography: Evidence from planktonic foraminiferal evolution, in *Evolution of the Cretaceous Ocean-Climate System*, edited by E. Barrera and C. C. Johnson, *Spec. Pap. Geol. Soc. Am.*, *332*, 301–328.

Premoli Silva, I., M. Caron, R. M. Leckie, M. R. Petrizzo, D. Soldani, and D. Verga (2009), *Paraticinella* n. gen. and taxonomic revision of *Ticinella bejaouaensis* Sigal, 1966, *J. Foraminiferal Res.*, *39*, 126–137, doi:10.2113/gsjfr.39.2.126.

Price, G. D. (1999), The evidence and implications of polar ice during the Mesozoic, *Earth Sci. Rev.*, *48*, 183–210, doi:10.1016/S0012-8252(99)00048-3.

Rabinowitz, P. D., and J. LaBrecque (1979), The Mesozoic South Atlantic and evolution of its continental margins, *J. Geophys. Res.*, *84*, 5973–6002.

Railsback, L. B., T. F. Anderson, S. C. Ackerly, and J. L. Cisne (1989), Paleoceanographic modeling of temperature-salinity profiles from stable isotopic data, *Paleoceanography*, *4*, 585–591, doi:10.1029/PA004i005p00585.

Robaszynski, F. and M. Caron (1995), Foraminifères planktoniques du Crétacé: Commentaire de la zonation Europe-Mediterranée, *Bull. Soc. Geol. Fr.*, *166*, 681–692.

Royer, D. L. (2006), $CO_2$-forced climate thresholds during the Phanerozoic, *Geochim. Cosmochim. Acta*, *70*, 5665–5675, doi:10.1016/j.gca.2005.11.031.

Sellwood, B. W., G. D. Price, and P. J. Valdes (1994), Cooler estimates of Cretaceous temperatures, *Nature*, *370*, 453–455, doi:10.1038/370453a0.

Sexton, P. F., P. A. Wilson, and R. D. Norris (2006), Testing the Cenozoic multisite composite $\delta^{18}O$ and $\delta^{13}C$ curves: New monospecific Eocene records from a single locality, Demerara Rise (Ocean Drilling Program Leg 207), *Paleoceanography*, *21*, PA2019, doi:10.1029/2005PA001253.

Shackleton, N. J., and J. P. Kennett (1975), Paleotemperature history of the Cenozoic and the initiation of Antarctic glaciation: Oxygen and carbon isotope analysis in DSDP sites 277, 279, and 280. *Initial Rep. Deep Sea Drill. Proj.*, *29*, 743–755.

Topper, R. P. M., R. Flecker, P. Meijer, and M. J. R. Wortel (2011), A box model of the Late Miocene Mediterranean Sea: Implications from combined $^{87}Sr/^{86}Sr$ and salinity data, *Paleoceanography*, *26*, PA3223, doi:10.1029/2010PA002063.

Trabucho Alexandre, J., R. I. van Gilst, J. P. Rodríguez-López, and P. L. de Boer (2011), The sedimentary expression of oceanic anoxic event 1b in the North Atlantic, *Sedimentology*, *58*, 1217–1246, doi:10.1111/j.1365-3091.2010.01202.x.

Tucholke, B. E., and P. R. Vogt (1979), Western North Atlantic sedimentary evolution and aspects of tectonic history, *Initial Rep. Deep Sea Drill. Proj.*, *43*, 791–825.

Ufnar, D. F., L. A. González, G. A. Ludvigson, R. L. Brenner, and B. J. Witzke (2004), Evidence for increased latent heat transport during the Cretaceous (Albian) greenhouse warming, *Geology*, *32*, 1049–1052, doi:10.1130/G20828.1.

Waelbroeck, C., et al. (2009), Constraints on the magnitude and patterns of ocean cooling at the Last Glacial Maximum, *Nat. Geosci.*, *2*, 127–132, doi:10.1038/ngeo411.

Weissert, H., and A. Lini (1991), Ice age interludes during the time of Cretaceous greenhouse climate?, in *Controversies in Modern Geology*, edited by D. W. Müller, J. A. McKenzie, and H. Weissert, pp. 173–191, Academic, London.

White, T., L. González, G. Ludvigson, and C. Poulsen (2001), Middle Cretaceous greenhouse hydrologic cycle of North America, *Geology*, *29*, 363–366, doi:10.1130/0091-7613(2001)029xxx0363:MCGHCOxxx2.0.CO;2.

Woo, K.-S., T. F. Anderson, L. B. Railsback, and P. A. Sandberg (1992), Oxygen isotope evidence for high-salinity surface seawater in the mid-Cretaceous Gulf of Mexico: Implications for warm, saline deepwater formation, *Paleoceanography*, *7*, 673–685, doi:10.1029/92PA01824.

Zachos, J. C., L. D. Stott, and K. C. Lohmann (1994), Evolution of Early Cenozoic marine temperatures, *Paleoceanography*, *9*, 353–387, doi:10.1029/93PA03266.

Zhou, J., C. J. Poulsen, D. Pollard, and T. S. White (2008), Simulation of modern and middle Cretaceous marine $\delta^{18}O$ with an ocean–atmosphere general circulation model, *Paleoceanography*, *23*, PA3223, doi:10.1029/2008PA001596.

D. R. Gröcke, Department of Earth Sciences, Durham University, Durham DH1 3LE, UK.

B. T. Huber, Smithsonian National Museum of Natural History, Washington, DC 20013, USA. (huberb@si.edu)

M. Kucera, Fachbereich Geowissenschaften, Eberhard-Karls Universität Tübingen, Hölderlinstrasse 12, DE-72076 Tübingen, Germany.

K. G. MacLeod, Department of Geological Sciences, University of Missouri, Columbia, MO 65211, USA.